MULTI-CHANNEL ALL-OPTICAL SIGNAL PROCESSING

by

LU LI

Presented to the Faculty of the Graduate School of

The University of Texas at Arlington in Partial Fulfillment

of the Requirements

for the Degree of

DOCTOR OF PHILOSOPHY

THE UNIVERSITY OF TEXAS AT ARLINGTON

August 2016

For my dear parents and
my fianc é Shuhan

ACKNOWLEDGEMENTS

First and foremost, I would like to thank my advisor, Dr. Michael Vasilyev for inspiring and supporting me during my PhD research work. His great insights and step-by-step guidance lead me into the field of fiber-optic communication. He is extremely patient and helpful during my Ph. D. study and research. His rigorous academic attitude, deep understanding and creative thinking have given me great influences.

I want to thank Dr. T. I. Lakoba from University of Vermont, who is collaborating with us in the research work. I also thank Young and Brandon for their collaboration and help on several projects and other group members, including Rouf, Afshin, Subrata and Kamanashis. Thanks to my former lab members Dr. Sarath Samudrala, Dr. Lei Zhu and Dr. Muthu Annamalai for their helpful discussions and suggestions.

I would like to thank members on my committee, Profs. R. Magnusson, J.C Chiao, W. Zhou and Y. Sun for their time and interest in my dissertation. I would also like to express my gratitude to Gail Paniuski and Janice Moore for their support and prompt response to all my administrative queries.

I would like to express my sincere and immense gratitude to my parents for their enduring supports and loves. I would give special thanks to my aunts, uncles and cousins, who provide lots of supports and helps while I chase my dream. At

last, I want to thank my fiancée, Shuhan. This PhD would not come true without her encouragement and support. This dissertation is dedicated to her and my parents.

June 23, 2016

ABSTRACT

MULTI-CHANNEL ALL-OPTICAL SIGNAL PROCESSING

Lu Li, PhD

The University of Texas at Arlington, 2016

Supervising Professor: Michael Vasilyev

We experimentally demonstrate, for the first time to our knowledge, a stand-alone all-optical regenerator capable of simultaneous 2R regeneration of multiple WDM channels.

Recently, our group has proposed an all-optical 2R regeneration scheme for multiple WDM channels [1]. This novel multi-channel regenerator is a modified configuration of Mamyshev 2R regenerator [2], in which a conventional highly-nonlinear-fiber (HNLF) is replaced by a novel group-delay-managed (GDM) nonlinear medium. The proposed multi-channel regeneration scheme uses multiple concatenated GDM unit cells, where each unit cell contains a piece of HNLF and a periodic-group-delay device (PGDD). Afterwards, the proof-of-principle experiment has also been demonstrated by using a recirculating loop to emulate of cascading multiple "fiber + PGDD" unit cells [3, 4]. However, the recirculating-loop-based regenerator is impractical and not useful in a real WDM systems. To make proposed regenerator practical, we build a GDM nonlinear medium with 4 or 6 "fiber + PGDD" unit cells, assisted by bi-directional Raman pumping.

In this dissertation, we build a stand-alone all-optical multi-channel regenerator and present our experimental results on 3-channel all-optical 2R regeneration with 100 GHz spacing and 200 GHz spacing, as well as 100-GHz-spaced 12- and 16-channel 2R regeneration. We first investigate 2R regeneration performance for 3 channels in a GDM nonlinear medium containing four "fiber + PGDD" unit cells in 200 GHz spacing case and 100 GHz spacing case. The experimentally observed

2 dB eye-opening improvement confirms that few-channel performance is not degraded by narrower 100 GHz channel spacing. Then, the 100-GHz-spaced multi-channel regeneration experiments were performed with as many as 12 channels (12 × 10 Gb/s), and, further, 16 channels (16 × 10 Gb/s) by employing a GDM medium with 6 unit cells. All 16 channels demonstrate eye-opening improvement better than 5 dB at BER level of 10^{-9}.

In addition, we make investigations of a nonlinear-optical-loop-mirror (NOLM) based all-optical regenerator that can be used in phase-encoded systems. We experimentally demonstrate, for the first time to our knowledge, a NOLM-based phase-preserving amplitude regeneration of high-duty-cycle (50%) RZ-DPSK signals degraded by amplitude jitter and amplified spontaneous emission (ASE) noise, confirmed by a 1.5 dB eye-opening improvement.

To show the path to extending the multi-channel regeneration capability to more advanced modulation formats, we propose a novel all-optical scheme of 16-QAM signal regeneration. The scheme consists of phase-sensitive amplifiers (PSAs), which are used to de-multiplex two quadratures, and new 2R regenerators, which are used for two-level amplitude signals. In the simulation, the capability of the regenerator has been demonstrated by constellation analysis. The modeling results show regenerated out signals have more than 4 dB signal-to-noise ratio (SNR) improvement on all 16 states compared to the degraded input signals.

TABLE OF CONTENTS

LIST OF ILLUSTRATIONS

CHAPTER 1

INTRODUCTION

As optical signal propagates in optical fibers, its strength becomes week due to the fiber attenuation. Then optical amplifiers are used to compensate the loss. The optical amplifiers add amplified spontaneous emission (ASE) noise to optical signals while amplifying them. After accumulation of ASE noise as well as other impairments in fiber communication lines, the degraded signal needs to be reset to its original shape to remove all noise and distortions for further transmission. This re-shaping process is called signal regeneration, which can be classified as: 1R (re-amplifying), 2R (re-amplifying + re-shaping), and 3R (re-amplifying + re-shaping + re-timing). It is achieved by employing either conventional electronic repeaters or all-optical regenerators. The electronic repeater consists of an optical transmitter-receiver pair and is based on opto-electro-opto (OEO) processing. It receives optical signal, converts it to electrical signal that is subsequently regenerated, and then uses this electrical signal to modulate another transmitter for re-transmission, which is quite complex. Moreover, electronic repeater or regenerator is inherently single-channel device, meaning that the same number of electric regenerators is required as the number of WDM channels, making the whole regeneration system very bulky, costly and power consuming. Moreover, electronic processing becomes extremely challenging when symbol rate is beyond 80 Gb/s, leaving all-optical regeneration the only option for signal regeneration.

Besides working with much higher (Terabit/s) maximum rates than their optoelectronic counterparts, all-optical regenerators can be data-rate independent and can simplify network management, which is also very advantageous. On the other hand, the electronic regenerators can offer more advanced capabilities (e.g., forward error correction) and lower manufacturing cost. Thus, to be practically viable, an all-optical regenerator must be less expensive, more compact and power efferent, which can be done only by processing many WDM channels in a single device to replace a large number of electronic regenerators. Therefore, compatibility with WDM channels becomes the most important challenge for all-optical regenerators [5, 6]. This challenge, however, is of fundamental nature. This is because strong optical nonlinearity is required for regenerators to form nonlinear power transfer function. This means that the cross-phase modulation (XPM) and four-wave mixing (FWM) interactions among the WDM channels are also taking place due to strong nonlinearity, which harms the WDM operation performance. While the re-timing function of 3R regenerator can, at least in principle, be performed for all WDM channels by a single device [7–9] (though under rather impractical assumptions of synchronized clock rates for all channels), the WDM operation of a 2R regenerator has remained a fundamental obstacle up until now.

Since multi-channel all-optical 2R regeneration is important yet challenging, the efforts on overcoming this problem have intensified over the last decade and people are trying different kinds of technologies to expand single-

channel regenerator to multi-channel case. They can be roughly arranged into three approaches: space-division multiplexing, polarization and bidirectional multiplexing, and using low-duty-cycle pulses (time-division multiplexing). The space-division multiplexing is to use spatial degrees of freedom to isolate WDM channels from interaction with each other. The incoming WDM channels are de-multiplexed into different fibers for a subsequent regeneration, which means it still requires many single-channel regenerators for multi-channel regeneration [8, 10–13]. Obviously, this technique does not take advantage of optical parallelism and cannot reduce regeneration cost per channel. The polarization and bidirectional multiplexing use other degrees of freedom, such as polarization [14] and opposite direction [15, 16] of propagation, to increase the number of channels for regeneration. However, it is limited by a small number of channels. For example, this approach has led to the demonstration of simultaneous regeneration of 4 channels in the same nonlinear fiber [17]. The low-duty-cycle or time-division multiplexing approach employs very low spectral efficiency in WDM transmission, which can help minimize interaction among the WDM channels either by placing the channels far from each other in frequency domain, or by separating the bits far from each other in time domain (i.e., using low-duty-cycle pulses). For the time-domain-separation method, the low duty cycle suppresses the interaction by ensuring that neighboring-channel pulses very rarely overlap in time.[18–20] For frequency-domain-spacing method, the interaction is suppressed by the presence of

substantial dispersion of the fiber, which makes the neighboring-channel pulse streams rapidly walk off from each other, thereby eliminating FWM and reducing XPM to merely a constant phase shift proportional to the average power of the neighboring channel. Since the dispersion also causes the different frequency components of the data-carrying pulses within each WDM channel to walk off from each other, this distorts the pulse shape and eliminates the regenerative effect of the optical nonlinearity unless the ratio of the bandwidth of each WDM channel to the inter-channel spacing, known as spectral efficiency, is very small. None of the three approaches discussed above has shown any potential for increasing the number of regenerated channels beyond 4, unless the channels carry identical data and are synchronized in time [21], which is impractical.

For multi-channel all-optical 2R regeneration, our group in collaboration with Prof. T. I. Lakoba from the University of Vermont proposed a scheme extending the principle of Mamyshev 2R regenerator [1] to arbitrary number of channels. It adapts Mamyshev regenerator to WDM operation by replacing the nonlinear medium with a group-delay-managed (GDM) nonlinear medium, consisting of several "fiber + periodic-group-delay device (PGDD)" unit cells. This novel nonlinear medium provides a special dispersion map that enables the accumulation of large amounts of self-phase modulation (SPM), which is beneficial for regeneration, while eliminating XPM and FWM interaction among WDM channels. The proposed multi-channel all-optical 2R regenerator has been

experimentally demonstrated for simultaneous 8 or 12-channel regeneration using a recirculating loop [3, 4], i.e., by placing one "fiber + PGDD" unit cell into a recirculating loop and letting the signals propagate through this cell multiple times to simulate many unit cells. Such recirculating loop regenerator was a great proof-of-principle demonstration, but was not a stand-alone device *per se*, and could not be used in a practical communication system. This dissertation focuses on building a stand-alone multi-channel all-optical regenerator without a recirculating loop on experimental demonstration of simultaneous 2R regeneration of multiple WDM channels. The first step is to investigate a few channels (3 channels in our case) with a relatively wide channel spacing (200-GHz) [22]. Then the number of channels increases to 12 and channel spacing decreases to 100-GHz [23]. Finally, we demonstrate GDM-based multi-channel 2R regenerator with 16-channel regeneration with 100-GHz spacing. Furthermore, to show the path to extending the multi-channel regeneration capability to more advanced modulation formats we study the phase-preserving amplitude regenerator in experiments and 16-QAM all-optical regenerator in simulation [24].

The structure of this dissertation is as follows. The second chapter gives an overview of nonlinear effects in optical fiber and fiber communication. In addition, it also gives introduction to all-optical regeneration, including amplitude regeneration and phase regeneration. In third chapter, we explain our proposed multi-channel all-optical 2R regenerator. We focus on the experimental setup and

results for simultaneous 3-, 12- and 16-channel 2R regeneration. In fourth chapter, we discuss another type of all-optical regenerator, which can be used in phase-encoded systems, its experimental setup and results. The fifth chapter describes a novel scheme for 16-QAM all-optical regeneration and preliminary numerical results. The last chapter discusses the future scope of this research work and summarizes the dissertation.

LU LI'S PUBLICATIONS/PRESENTATIONS

1. "Experimental demonstration of spatial-mode-selective frequency up-conversion in a multimode $\chi(2)$ waveguide,"

Y. B. Kwon, M. Giribabu, L. Li, S. C. Samudrala, C. Langrock, M. M. Fejer, and M. Vasilyev, *the Conference on Lasers and Electro-Optics*, San Jose, CA, June 5–10, 2016, paper STh3P.4.

2. "2R Regeneration of 12 WDM Channels with 100-GHz Spacing in a Group-Delay-Managed Nonlinear Medium,"

L. Li, K. Young, C. Brandon, T. I. Lakoba and M. Vasilyev, *the Optical Fiber Communication Conference*, Anaheim, CA, March 20–24, 2016, paper W4D.4. **Semi-finalist of the Corning Best Student Paper competition.**

3. "All-optical regeneration of multi-channel signals,"

L. Li and M. Vasilyev, *UT Arlington Photonics Symposium*, University of Texas at Arlington, Arlington, TX, September 14, 2015.

4. "Investigation of 3-Channel All-Optical Regeneration in a Group-Delay-Managed Nonlinear Medium,"

L. Li, M. Vasilyev, and T. I. Lakoba, *the Conference on Lasers and Electro-Optics*, San Jose, CA, May 10–15, 2015, paper SM2M.2. **Semi-finalist of the T. Maiman Best Student Paper competition.**

5. (Invited) "Experimental progress on multichannel regeneration in group-delay-managed nonlinear media,"

P. G. Patki, L. Li, M. Vasilyev, and T. I. Lakoba, *Aston Workshop on Multichannel Regeneration*, Aston University, Birmingham, United Kingdom, October 24, 2014.

6. "Phase noise suppression of a 50%-duty-cycle RZ-DPSK signal by using an attenuation-imbalanced NOLM,"

L. Li, M. Vasilyev, and T. I. Lakoba, *IEEE Summer Topical Meeting on Nonlinear-Optical Signal Processing*, Montréal, Québec, Canada, June 14–16, 2014. **Finalist of the Best Student Paper competition.**

7. "Nonlinear-optical-loop-mirror-based, phase-preserving 2R regeneration of a high-duty-cycle RZ-DPSK signal,"

L. Li, M. Vasilyev, and T. I. Lakoba, *the Conference on Lasers and Electro-Optics*, San Jose, CA, June 8–13, 2014, paper JW2A.13.

8. "All-optical 2R regenerator of 16-QAM signals,"

L. Li and M. Vasilyev, *the "Next-Generation Optical Communication: Components, Sub-Systems, and Systems III" conference (part of SPIE OPTO / Photonics West)*, February 1–6, 2014, San Francisco, CA, paper 9009-7; Proc. SPIE **9009**, 9009-7.

CHAPTER 2

OVERVIEW OF ALL-OPTICAL REGENERATION IN FIBERS

In the past century, optical fibers were developed to transmit data at a high capacity over a long distance due to their very low attenuation (<0.18 dB/km) and large bandwidth (>1 THz). With the increasing capacities, optical signals have a higher requirement on optical signal-to-noise ratio (OSNR) and become more sensitive to amplitude and phase noise, which means more frequent regenerations are needed along the transmission link. This chapter describes the properties of optical fibers and nonlinear effects that can be used to reshape the optical signal into its original forms.

2.1 Fiber Losses

The most important parameter for fibers, cables or any transmission media is the attenuation or loss, a measure of power loss during transmission. If P_{in} is the input power of a fiber of length L, the output power is given by

$$P_{\text{out}} = P_{\text{in}} \exp(-\alpha L), \tag{2.1}$$

where the attenuation constant α is used to measure the total fiber losses. α can be expressed in units of dB/km using the relation

$$\alpha = -\frac{10}{L}\log\left(\frac{P_{\text{out}}}{P_{\text{in}}}\right). \tag{2.2}$$

The beauty of optical fiber is its low loss, which makes it a perfect transmission medium for optical information carriers. A typical standard single-mode fiber

(SSMF) has a minimum loss of ~0.2 dB/km near 1550 nm. Fig. 2.1 shows the loss spectrum of a SSMF made in 1979. There are several contributions to the loss spectrum. Among them, material absorption and Rayleigh scattering are major factors. While Rayleigh scattering limits the use of wavelengths below 800 nm, the material absorption increases significantly above 1700 nm. In addition, the loss spectrum exhibits a strong peak near 1.39 μm and several other smaller peaks, originating from OH-ion vibrations. According to the loss spectrum, there are two low-loss windows: 1310 nm and 1550 nm. The O-band, or original band, covers 1260 nm to 1360 nm while C-band, or conventional band, covers 1530 nm to 1565 nm. Recently, the commercially available SSMFs have reached a maximum attenuation of 0.17 dB/km at 1550 nm and 0.31 dB/km at 1310 nm [25].

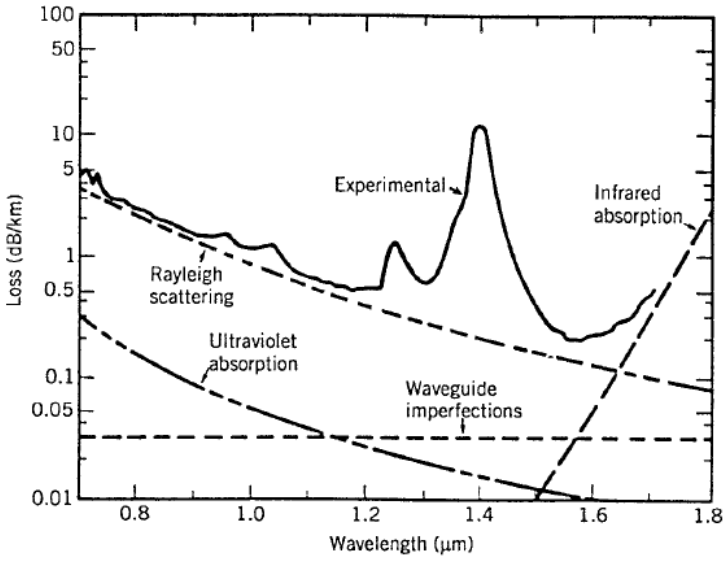

Fig. 2.1. Loss spectrum of a single-mode fiber produced in 1979.

(Revised from Ref. [26]).

2.2 Dispersion in Single-Mode Fibers

Optical fiber's refractive index is frequency-dependent, which is called chromatic dispersion. In another word, the light waves of different wavelengths travel in the fibers at different speeds, thus causing group delay between them. Therefore, fiber dispersion plays a critical role in the propagation of optical pulses, which have many different frequency components. If a pulse has a spectral width $\Delta\omega$, the pulse broadening ΔT for a fiber of length L is governed by

$$\Delta T = \frac{dT}{d\omega}\Delta\omega = \frac{d}{d\omega}\left(\frac{L}{\upsilon_g}\right)\Delta\omega. \tag{2.3}$$

Using $T = L / \upsilon_g$, where υ_g is the group velocity, defined as [27]

$$\frac{1}{\upsilon_g} = \left(\frac{d\beta}{d\omega}\right), \tag{2.4}$$

we find that ΔT is governed by

$$\Delta T = L\left(\frac{d^2\beta}{d\omega^2}\right)\Delta\omega = L\beta_2\Delta\omega, \tag{2.5}$$

where parameter $\beta_2 = d^2\beta / d\omega^2$ is known as the GVD parameter. It represents dispersion of the group velocity and is responsible for pulse broadening. In optical communications, another dispersion parameter D is more often used in practice, which is defined as

$$D = \frac{d}{d\lambda}\left(\frac{1}{\upsilon_g}\right) = -\frac{2\pi c}{\lambda^2}\beta_2, \tag{2.6}$$

where c is speed of light, and λ is the wavelength. Then ΔT can be also expressed in term of D,

$$\Delta T = \frac{d}{d\lambda}\left(\frac{L}{\upsilon_g}\right)\Delta\omega = DL\Delta\lambda. \tag{2.7}$$

Equation (2.7) is often used to calculate the group delay between different frequency components. Both β_2 and D are the parameters used to describe the dispersion. They have a different sign and are directly connected through equation (2.6). Both β_2 and D are wavelength dependent, so that there is possibility of $\beta_2 = D=0$ at a specific wavelength. That wavelength is called zero-dispersion wavelength and is denoted as λ_D. For a silica fiber, if wavelength $\lambda < \lambda_D$, then $\beta_2 > 0$ (or $D < 0$), the fiber is said to exhibit normal dispersion. If wavelength $\lambda < \lambda_D$, then $\beta_2 < 0$ (or $D > 0$), the fiber is said to exhibit anomalous dispersion. In the normal dispersion regime, short wavelength (blue-shifted) components of an optical pulse travel slower than long wavelength (red-shifted) components of the same pulse. By contrast, the opposite occurs in the anomalous dispersion regime in which $\beta_2 < 0$ (or $D > 0$). The zero-dispersion wavelength is a very important property of fibers. People have modified the λ_D of fibers for different purposes and applications. The anomalous-dispersion regime is of considerable interest for the study of nonlinear effects because it is in this regime that optical fibers support solitons through a balance between the dispersive and nonlinear effects.

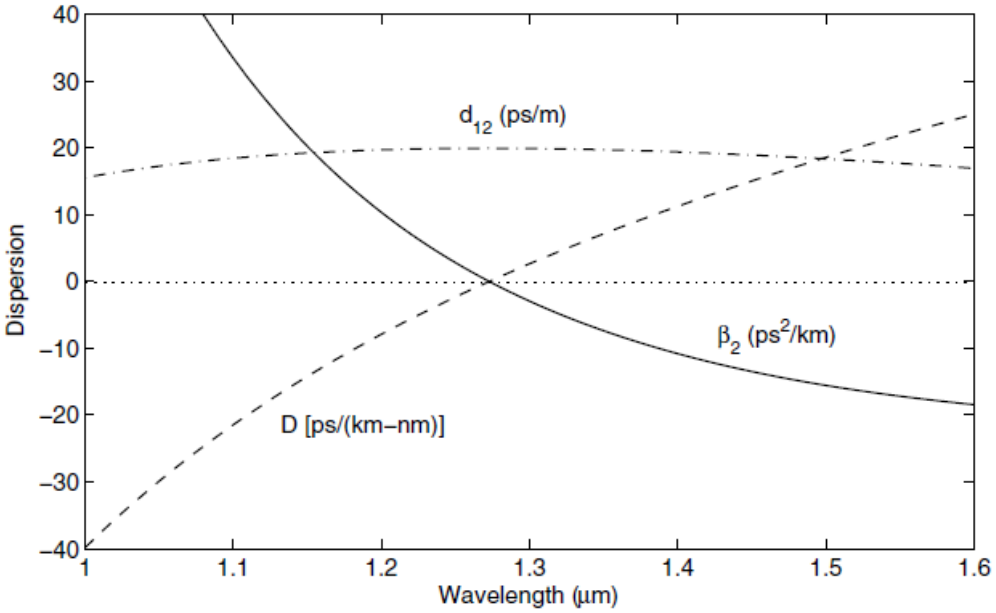

Fig. 2.2. Variation of *D* and β_2 with the wavelength for fused silica.

(Revised from Ref. [28])

2.3 Nonlinearities of Fiber

In optics, the term nonlinear propagation means that the properties of the medium depend on the strength of propagating optical field. In principle, any dielectric medium can behave like a nonlinear medium if the electromagnetic field is strong enough. Fundamentally, origin of nonlinearity relies on anharmonic motion of bound electrons under the influence of an applied field. The total polarization *P* induced by electric dipoles is not linear but satisfies more general relation as

$$P = \varepsilon_0\left(\chi^{(1)} \cdot E + \chi^{(2)} : E^2 + \chi^{(3)} \vdots E^3 + \cdots\right), \tag{2.8}$$

where ε_0 is the permittivity of vacuum and $\chi^{(k)}$ (k = 1, 2, . . .) is the kth order susceptibility. In optical fiber, the second $\chi^{(2)}$ term becomes zero, since its material SiO_2 is centro-symmetric. Therefore optical fibers do not exhibit second-order nonlinear effects, and the lowest-order nonlinear effects in fibers originate from third-order susceptibility $\chi^{(3)}$. Such a medium as silica is called a Kerr medium and it manifests the power dependence of the refractive index, responsible for the Kerr effect. The simple form of refractive index can be written as

$$n(I) = n_0 + n_2 \cdot I, \tag{2.9}$$

where n_0 is the linear refractive index, n_2 is the nonlinear-index coefficient, and I is the optical intensity. The higher-order terms may exist, but are neglected here. According to chapter 2 in Ref. [29], the nonlinear-index coefficient can be written as

$$n_2 = \frac{2}{\varepsilon_0 c n} \frac{3}{8} \mathrm{Re}(\chi^{(3)}_{xxxx}), \tag{2.10}$$

where c is the speed of light in vacuum. We will discuss three different Kerr effects in this chapter: Self-Phase Modulation (SPM), Cross-Phase Modulation (XPM) and Four-Wave Mixing (FWM).

The nonlinear effects grow with propagation distance. For a longer fiber link, more light-matter interaction occurs, leading to stronger nonlinear effects. On the other hand, due to the fiber loss, the light intensity decreases according along the

fiber length. Therefore, the effective length L_{eff} is often used in nonlinear optics. For an actual fiber length L, its effective length is defined as,

$$P_{\text{in}} L_{\text{eff}} = \int_{z=0}^{L} P(z)dz, \tag{2.11}$$

where z is the distance, P_{in} is the input power at $z = 0$. Using the optical power $P(z)$ at the distance z alone the link (see equation (2.1)), the effective length L_{eff} is obtained as,

$$L_{\text{eff}} = \frac{1-\exp(-\alpha z)}{\alpha}. \tag{2.12}$$

In the case of no amplification, $L_{\text{eff}} \approx 1/\alpha$ when the fiber length is very long.

In addition, the nonlinear effects also depend on the light intensity in fiber and the intensity is inversely proportional to the area of the core. The effective cross-sectional area A_{eff} is always used and can be expressed as

$$A_{\text{eff}} = \frac{\left(\iint_{-\infty}^{+\infty} |F(x,y)|^2 dxdy \right)^2}{\iint_{-\infty}^{+\infty} |F(x,y)|^4 dxdy}, \tag{2.13}$$

where $F(x,y)$ is the transverse profile of the fiber mode. For single-mode fibers, equation (2.13) can be simplified as,

$$A_{\text{eff}} = \frac{\pi}{4}(\text{MFD})^2, \tag{2.14}$$

where MFD is mode-field diameter. For example, the effective area for the fundamental mode propagating in the standard single-mode fiber is ~ 80 μm^2 with

MFD = 10 μm. Then, in terms of n_2 and A_{eff}, the nonlinear parameter γ can be expressed as,

$$\gamma(\omega_0) = \frac{\omega_0 n_2}{c A_{\text{eff}}}. \tag{2.15}$$

The value of γ ranges from 1 to 30 $W^{-1}km^{-1}$ depending on the fiber type and wavelength.

2.3.1 Self-Phase Modulation (SPM)

One of the most common Kerr effects is self-phase modulation. The different portions of a light pulse experience different amounts of phase shift due to power-dependent refractive index. The SPM-induced phase shift φ_{SPM} is given by [29],

$$\varphi_{\text{SPM}}(t) = \gamma L_{\text{eff}} P(t), \tag{2.16}$$

where $P(t)$ is the pulse's power within its duration. The equation (2.16) shows time-dependent phase shift, meaning different parts of a pulse undergo different SPM phase shifts. The time dependence of φ_{SPM} is responsible for change in frequency spectrum. The difference δω is given by,

$$\delta\omega = -\frac{\partial \varphi_{\text{SPM}}(t)}{\partial t} = -\gamma L_{\text{eff}} \frac{\partial P(t)}{\partial t}. \tag{2.17}$$

2.3.2 Cross-Phase Modulation (XPM)

In addition to SPM, another consequence of intensity-dependent refractive index is cross-phase modulation (XPM). When two or more optical beams propagate together in a fiber, there can be an XPM-induced nonlinear phase change in each beam, because the nonlinear refractive index depends not only on the intensity of

that beam but also on the intensity of the other co-propagating beams. The XPM effect is always accompanied with SPM effect. Therefore, the nonlinear phase shift for the *i*th signal in the fiber with two or more optical signals is given by [28]

$$\varphi_{NL,i} = \gamma L_{\text{eff}} \left(P_i + 2\sum_{j \neq i} P_j\right). \tag{2.18}$$

The first term on right side of equation (2.18) is represents SPM-induced phase shift, which originates from the *i*th-signal's own intensity dependence. The second term represents XPM-induced phase shift, which comes from the interaction with the other signals. It is worth to mention that XPM effect is two times stronger than SPM (factor of 2 in the above equation), but it is only true when beams have the same polarization. The XPM effect has the same strength as the SPM effect when beams have orthogonal polarizations. In a WDM system, XPM becomes the major impairment and damages the system performance more than the SPM. The influence of the XPM effect intensifies with increasing number of channels. The result of XPM may be asymmetric spectral broadening and distortion of the pulse shape [28]. However, the XPM between channels spaced far from each other in frequency can be washed out due to their pulses' walk-off in the presence of dispersion, which leaves the phase shift (2.18) that depends only on the average, not instantaneous, power of the other channel.

2.3.3 Four-Wave Mixing (FWM)

Another phenomenon resulting from the Kerr effect is four-wave mixing (FWM). FWM is a nonlinear process by which signals at different wavelengths are mixed together to produce new signals at new wavelengths. Fig. 2.3 shows that two optical signals at frequencies ω_1 and ω_2, through FWM process, generate two sideband signals at new frequencies ω_3 and ω_4. The four frequencies satisfy the following relationship,

$$\omega_3 + \omega_4 = \omega_1 + \omega_2 . \tag{2.19}$$

In the language of quantum mechanism, two photons at frequencies ω_1 and ω_2 are annihilated, while two photons at frequencies ω_3 and ω_4 are created simultaneously.

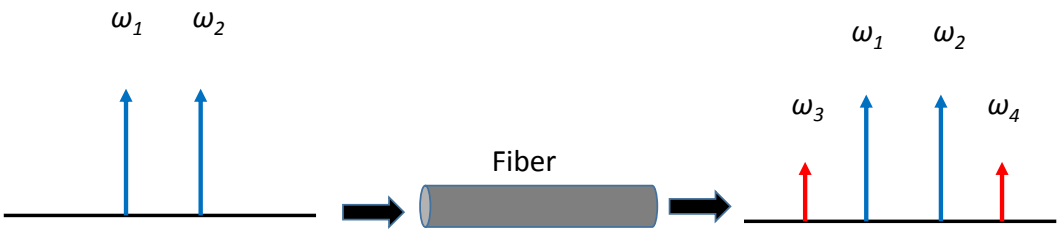

Fig. 2.3. Diagram of four-wave mixing

The main features of FWM can be understood from the third-order polarization term in equation (2.8),

$$P_{\mathrm{NL}} = \varepsilon_0 \chi^{(3)} \vdots E^3 . \tag{2.20}$$

Assuming that all waves have the same linear polarization, the total electric field can be written as,

$$E = \frac{1}{2}\sum_{j=1}^{4} E_j \exp[i(\beta_j z - \omega_j t)] + c.c., \tag{2.21}$$

where the propagation constant $\beta_j = n_j \omega_j / c$. Substituting equation (2.21) into equation (2.20) and using nonlinear parameter γ, one of four waves (P_4) can be expressed as,

$$P_4 = \gamma[|E_4|^2 E_4 + 2(|E_1|^2 + |E_2|^2 + |E_3|^2)E_4 + 2E_1E_2E_3\exp(i\theta_+) + 2E_1E_2E_3^*\exp(i\theta_-) + \cdots],$$

(2.22)

where θ_+ and θ_- are defined as

$$\theta_+ = (\beta_1 + \beta_2 + \beta_3 - \beta_4)z - (\omega_1 + \omega_2 + \omega_3 - \omega_4)t, \tag{2.23}$$

$$\theta_- = (\beta_1 + \beta_2 - \beta_3 - \beta_4)z - (\omega_1 + \omega_2 - \omega_3 - \omega_4)t. \tag{2.24}$$

The first four terms containing E_4 in equation (2.22) are responsible for the SPM and XPM effects, but the remaining terms result from the frequency combinations (sum or difference) of all four waves.

There are two types of FWM terms in equation (2.22). The term containing θ_+ corresponds to the case in which three photons transfer their energy to a single photon at the frequency $\omega_4 = \omega_1 + \omega_2 + \omega_3$. This term is responsible for the phenomena such as third-harmonic generation ($\omega_1 = \omega_2 = \omega_3$). In general, it is difficult to satisfy the phase-matching condition for such processes to occur in optical fibers with high efficiencies. The term containing θ_- in equation (2.22) corresponds to the case of FWM. The phase-matching requirement for this process is $\Delta k = 0$, where

$$\Delta k = \beta_3 + \beta_4 - \beta_1 - \beta_2 . \tag{2.25}$$

SPM and XPM are significant mainly for high bit-rate systems, but the FWM effect is independent of the bit rate and is critically dependent on the channel spacing and fiber dispersion. Decreasing the channel spacing increases the four-wave mixing effect and so does decreasing the dispersion. FWM has been recognized as one of the limiting factors in the design of high-performance WDM optical transmission links with a large number of channels. In the case of equally spaced channels, the new frequencies coincide with the existing frequencies leading to in-band crosstalk. When channels are not equally spaced, most FWM generated components fall in between the channels and leads to crosstalk, which does not degrade the system performance as severely as in-band crosstalk. However, in both cases, in addition to the crosstalk interference, the depletion of the original signal waves can severely degrade multi-channel system performance.

2.4 All-Optical Regenerators

2.4.1 Mamyshev regenerator

One of the most popular all-optical regenerators is the Mamyshev regenerator, which is used to regenerate On-Off Keying (OOK) signal [2]. The schematic of Mamyshev regenerator is shown in Fig. 2.4. It consists of two components: a nonlinear medium (e.g., highly nonlinear fiber, or HNLF) and an optical bandpass filter (OBPF).

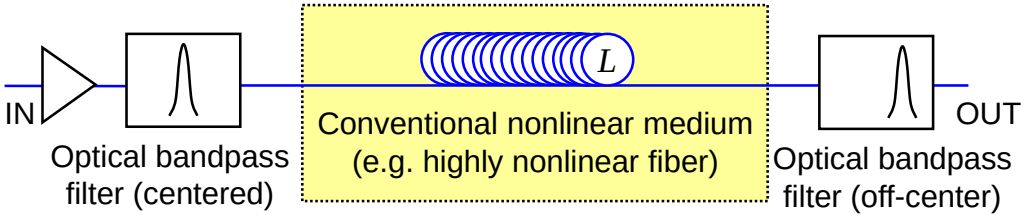

Fig. 2.4. Schematic diagram of Mamyshev regenerator

The operation of Mamyshev regenerator is illustrated in Fig. 2.5 for the case of a single channel. Assuming that a noisy input pulse ("ONE" symbol) has a full width half maximum (FWHM) spectral bandwidth $\Delta\nu_0$, it experiences SPM-caused spectral broadening during its propagation in the HNLF. The nonlinear phase shift is given by:

$$\Delta\nu_{\mathrm{NL}} = \Delta\nu_0 \gamma P_0 L_{\mathrm{eff}}\,, \tag{2.26}$$

where P_0 is the input pulse peak power, γ is the nonlinear coefficient, and L_{eff} is the effective length of HNLF. For large input power when $\Delta\nu_{\mathrm{NL}} >> \Delta\nu_0$, the spectral density at the HNLF output has almost constant height and becomes independent of the input pulse's peak power P_0. Only width of the broadened spectrum $\Delta\nu_{\mathrm{NL}}$ is proportional to the input peak power. Hence, the output power from the OBPF is also independent of input pulse's peak power and proportional to the width of the OBPF. If OBPF width $\Delta\nu_f \approx \Delta\nu_0$, one can obtain an output pulse of approximately the same duration as the input pulse, but input power fluctuations will not transfer into output signal, which constitutes the regeneration of "ONES" symbols. On the other hand, any noise between the pulses (i.e., taking place of "ZERO" symbols) is

too weak to cause SPM broadening and is confined within the input signal's bandwidth. If the OBPF center frequency is offset from the center of the input signal's spectrum, the noise between the pulses is not transmitted to filter's output, which constitutes the regeneration of "ZERO" symbols.

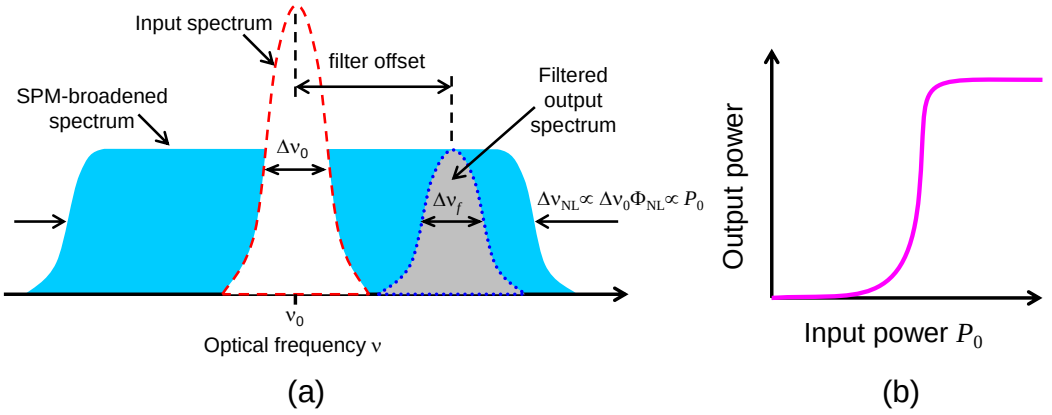

Fig. 2.5. Operation principle of Mamyshev regenerator

From the discussion above, we know that the Mamyshev scheme requires strong nonlinearity to ensure large amount of SPM for optical regeneration. However, the nonlinearity also causes strong interaction, such as cross-phase modulation, between the neighboring channels, which degrades the multi-channel operation and eventually destroys regeneration. As a result, regular Mamyshev regenerator will not work for simultaneous regeneration of multiple WDM channels. We proposed a scheme that can adapt Mamyshev regenerator to a multi-channel 2R regenerator, in which the conventional HNLF is replaced by a novel artificial nonlinear medium. This part will be discussed in the next chapter.

2.4.2 Phase-preserving amplitude regenerators

As we discussed previously, PSAs have the capability of improving the quality of phase-encoded modulation formats (e.g., DPSK) through regenerating phase directly. However, there is an alternative regenerator that could be used with such signals and can regenerate amplitude without disturbing the phase, called phase-preserving amplitude regenerator. Compared to PSAs, even though not regenerating the phase *per se*, such regenerators are still very useful in phase-encoded systems. This is because they do signal quality improvement in a simpler and cheaper way: they suppress nonlinear conversion of amplitude noise to phase noise, which is called Gordon-Mollenauer effect and is the main impairment of the phase-encoded systems. Several phase-preserving amplitude regenerator schemes have been recently introduced [30–33]. Among them, we think that the regenerator based on asymmetric nonlinear optical loop mirror (NOLM) [30, 31] is the most promising one because of its potential of regenerating multiple WDM channels simultaneously by employing a special group-delay-managed nonlinear medium [34].

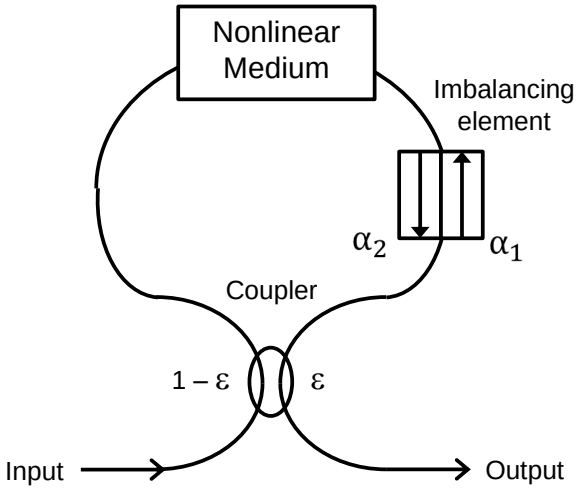

Fig. 2.6. Schematic diagram of NOLM-based regenerators

A NOLM-based phase-preserving amplitude-regenerating device usually consists of three basic elements: a nonlinear medium (e.g., HNLF), a highly-asymmetric coupler and an imbalancing element, which could be amplifier, attenuator, or, in our case, directional attenuator (DA). Fig. 2.6 shows the schematic diagram of a typical NOLM-based regenerator. Signal regeneration by a NOLM is based on constructive and destructive interference. An incoming pulse is split by a coupler with the asymmetric splitting ratio into two counterpropagating pulses with different power levels, which propagate through a fiber loop clockwise and anti-clockwise, respectively. According to their power levels, the pulses gather different amounts of SPM phase shifts before they interfere at the coupler. Therefore, the output power can be expressed by equation (2.27) and phase expression given by equation (2.28):

$$P_{\text{out}} = P_{\text{in}}\{\alpha_2(1-\varepsilon)^2 + \varepsilon^2 - 2\alpha_2\varepsilon(1-\varepsilon)\cos[\varphi_{\text{NL}}(2\varepsilon-1)]\}, \tag{2.27}$$

$$\varphi_{out} = -\arctan\frac{\varepsilon\sin(\alpha\varphi_{NL}) - \sqrt{\alpha_2}(1-\varepsilon)\sin[(1-\varepsilon)\varphi_{NL}]}{\varepsilon\cos(\alpha\varphi_{NL}) - \sqrt{\alpha_2}(1-\varepsilon)\cos[(1-\varepsilon)\varphi_{NL}]}. \tag{2.28}$$

Here P_{out} is the output power, P_{in} the input power, ε the coupling ratio, α_1 and α_2 are gain/loss factor clockwise and anti-clockwise. The $\varphi_{NL} = \gamma L P_{in}$ represents the nonlinear phase shift in the nonlinear medium. The two equations lead to a nonlinear power (bottom in Fig. 2.7) and phase (top in Fig. 2.7) transfer characteristic curve. The characteristic shows a flattened region (the shadowed blue area in Fig. 2.7), where amplitude fluctuations ΔP_{in} are suppressed effectively so that $\Delta P_{out} < \Delta P_{in}$. Meanwhile, the phase is not changed after amplitude regeneration, according to the phase transfer curve.

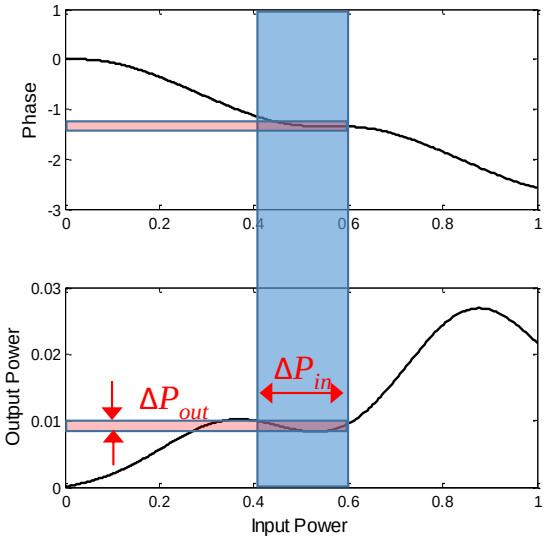

Fig. 2.7. Phase (upper) and power (bottom) transfer curve of NOLM

However, so far the experimental demonstrations of NOLM-based phase-preserving amplitude regenerators have only used pulses with relatively low duty

cycle (< 8%), which have low spectral efficiency and are impractical. The difficulties in using high-duty-cycle pulses is that XPM phase shift could cancel the beneficial SPM phase shift. XPM between the counter-propagating beams shifts the bias point of the NOLM interferometer. For low-duty-cycle RZ pulses, XPM phase shift is very small and its impact can be negligible. As the duty cycle increases, the plateau in input-output power transfer curve shifts toward higher and higher powers. When duty cycle reaches 50%, XPM completely cancels the beneficial SPM. However, the impact of this XPM can be counteracted by a linear phase bias, which can be introduced by playing with polarization or using an acousto-optic frequency shifter placed asymmetrically in the loop. In our case, we use polarization controllers to adjust the linear phase bias of the NOLM, which will be discussed in chapter 4.

CHAPTER 3

A STAND-ALONE MULTI-CHANNEL ALL-OPTICAL REGENERATOR

One of the main reasons why nonlinear-optical signal regeneration has not yet become a practical alternative to electronic processing is that the all-optical elements with nonlinear input-output relationship have remained inherently single-channel and, hence, cannot fully utilize the parallel processing potential of optical fibers and amplifiers. In this chapter, we discuss our solution to this problem: an optical signal processor employing a novel GDM nonlinear medium where strong SPM is achieved without such nonlinear crosstalk, and demonstrate, for the first time, simultaneous all-optical regeneration of up to 16 WDM channels by one device.

3.1 Multi-channel Mamyshev regenerator based on GDM nonlinear medium

As we discussed in chapter 2, Mamyshev regenerator does not work with WDM channels due to nonlinear crosstalk among channels. The all-optical regeneration working with multi-channel (number of channel >6) has not yet been achieved, though its demand is urgent. Then, a radically different method of WDM regeneration was proposed by our group in collaboration with Prof. T. I. Lakoba from the University of Vermont in [1]. This approach uses the benefits of the dispersive walk-off between the WDM channels to avoid FWM and XPM, but at the same time eliminates the walk-off among the frequency components within each channel to preserve pulse integrity and enable accumulation of large amounts

of SPM. In order to adapt Mamyshev regenerator to WDM operation, the HNLF in Mamyshev regenerator is divided into several small pieces, separated by periodic-group-delay devices (PGDDs), as shown in Fig. 3.1. Those PGDDs are nothing but spectrally-periodic phase filters, which are made of several cascaded Gires-Tournois etalons and have sawtooth-like group-delay spectra. Each section of HNLF and PGDD form a unit cell and several unit cells combine into the group-delay-managed (GDM) nonlinear medium.

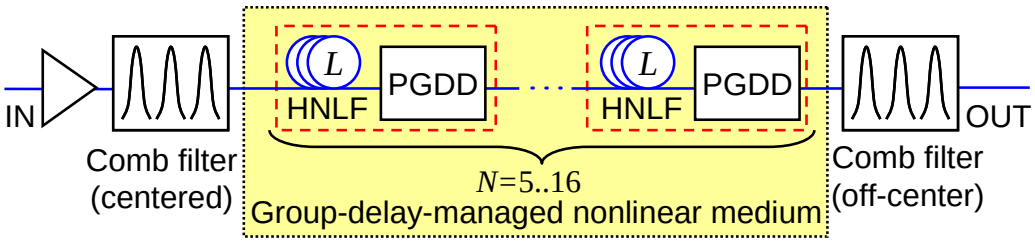

Fig. 3.1. Schematic of our proposed multi-channel Mamyshev regenerator

Here, the HNLF provides nonlinearity for SPM and large negative dispersion or a straight-line with negative slope group-delay spectrum in Figure 3.2, where the spectrum of the "fiber + PGDD" unit cell exhibits staircase-like behavior. This novel dispersion map ensures equal delays among all frequency components within each channel, thereby maximizing SPM, but at the same time introduces temporal walk-off between different WDM channels for XPM and FWM suppression. Figure 3.3 shows that, when multiple "fiber + PGDD" unit cells are concatenated, the walk-off is accumulated, effectively resulting in the creation of a new artificial nonlinear medium with large group velocity dispersion among different WDM

channels and with no dispersion within each channel. By employing the GDM nonlinear medium, the benefits of large SPM can be enjoyed simultaneously by each of many WDM channels without suffering from the FWM and XPM. In the future, it might be possible to implement the entire GDM on a chip using integrated-photonics solutions for both nonlinear [35, 36] and PGDD [37–39] functions.

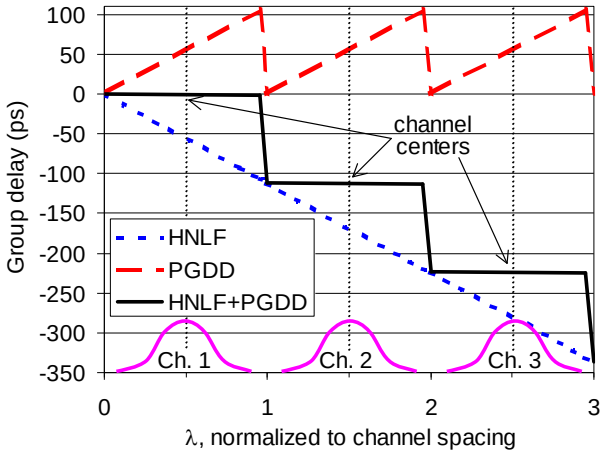

Fig. 3.2. Group delay map of "fiber + PGDD" unit cell

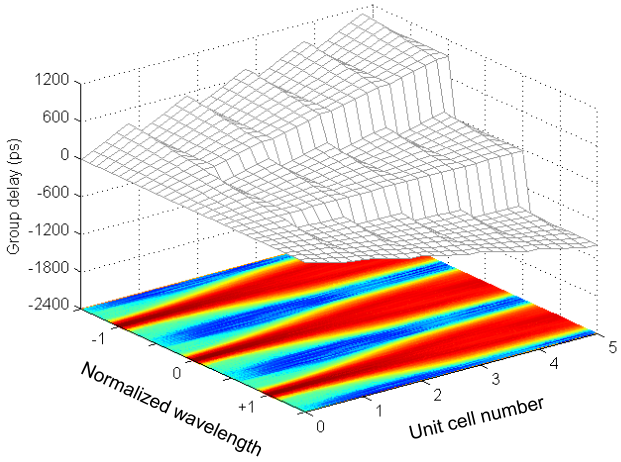

Fig. 3.3. Group delay map of cascaded "fiber + PGDD" unit cells

The idea of using dispersive delay to suppress XPM was originally proposed for conventional long-haul communication lines [40, 41] and later was demonstrated with PGDDs for dispersion-managed soliton transmission [42, 43]. The long-haul communication lines, however, operate in the regime where the nonlinearities are weak, whereas 2R regeneration inherently relies on large SPM. We found the optimum parameters of operation for the latter regime [44], which indicate that the desired 2R performance can be obtained with as few as 5 or 6 "fiber + PGDD" unit cells with anomalous net dispersion of the cell and large normal dispersion of the nonlinear fiber.

3.2 Three-channel Optical Regeneration Experiment

3.2.1 Group-Delay-Managed Nonlinear Medium

The key part of our multi-channel regeneration experiment is the group-delay-managed (GDM) nonlinear medium. As shown in Fig. 3.4, the GDM nonlinear medium contains 4 unit cells in three-channel regeneration experiment. Each of them consists of a 1-km-long section of DCF, instead of HNLF mentioned in chapter 2, and one PGDD. The DCF has a dispersion of –120 ps/nm/km. According to Prof. Lakoba's previous modeling, the unit cell should have a positive residual dispersion to enhance the regeneration. Thus, the dispersion of each PGDD is set to +135 ps/nm in order to have the optimum residual dispersion of +15 ps/nm for each unit cell. The PGDD has a loss of 3.8–4 dB. In addition to that, there are other losses from DCF, WDM combiners/splitters and SMF to DCF splicing,

contributing to the total loss of 25.5 dB. To compensate the loss of the whole transmission link, four Raman Pump Units (RPUs) are used to bi-directionally pump the GDM medium to transparency. Each of RPUs has two wavelengths of 1440 nm and 1450 nm and two polarizations multiplexed, while four additional 1450/1550 nm pump/signal WDM combiners/splitters are inserted to make the Raman pump light bypass the lossy PGDDs.

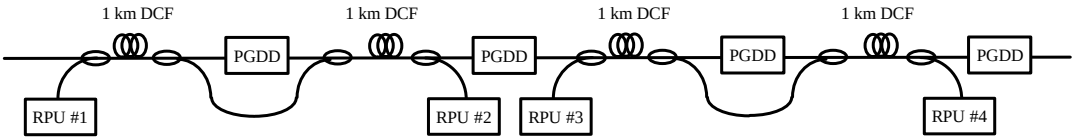

Fig. 3.4. GDM nonlinear medium for 3-channel regeneration

3.2.2 Three-channel Experimental Setup

Figure 3.5 shows the schematic of three-channel regeneration experiment using GDM nonlinear medium. The signals are generated either in three 200-GHz-spaced odd ITU channels, which are 1550.92 nm, 1552.52 nm and 1554.13 nm, or in three 100-GHz-spaced channels by interleaving one odd (1552.52 nm) and two even ITU channels (1551.72 nm and 1553.33 nm). All signals are OOK-modulated at 10.7 Gb/s by a 2^{31}–1 pseudo-random bit sequence (PRBS) and carved into 50% RZ pulses. Another modulator is driven by a 1-GHz sine wave from an independent source to emulate a large (±35%) amplitude jitter. This frequency is chosen to be far beyond the bandwidth of Raman cross-gain saturation in 2-km-long amplifiers used below. After the first EDFA, 1.25-km DCF (nonlinearity $\gamma = 5\ W^{-1}km^{-1}$)

ensures 2.4-bit delay between the adjacent 200-GHz-spaced channels (1.2-bit delay between 100-GHz-spaced channels), decorrelating their PRBS bit patterns. Most of the out-of-band ASE is suppressed by a cascade of a 4-nm-wide optical bandpass filter (OBPF) and a 50-to-100 GHz interleaver with 0.25-nm-wide passband. After the second, high-power, EDFA the co-polarized signals enter Mamyshev regenerator based on the GDM nonlinear medium. The total average power entering the GDM medium is 21.5 dBm (~50 mW / channel). The average output power of the last 1-km DCF section is 22 dBm, which indicates nearly uniform nonlinearity distribution among different 1-km DCF sections. Then, a 0.2-nm-wide OBPF is set to –0.09-nm off the center wavelength of signals to cut a portion of SPM-broadened spectrum. For a practical use in a WDM system, it can be replaced by a comb filter to achieve simultaneous regeneration for all WDM channels. Afterwards, all channels are characterized by a pre-amplified receiver.

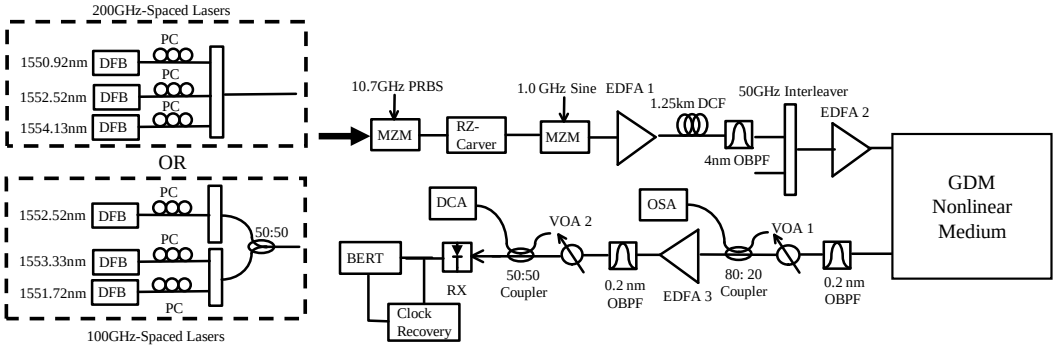

Fig. 3.5. Experimental setup for three-channel regeneration

3.2.3 200-GHz-Spaced Three-channel Results

Figure 3.6 shows the eye diagrams of the regenerator input and output signals for 200-GHz spacing case. Figure 3.6 (a) illustrates the back-to-back signal without noise and Figure 3.6 (b) shows the input signal degraded by ±35% amplitude jitter. The amplitude-jitter-degraded signal after regeneration is shown in Figs. 6 (c)–(e) for the three 200-GHz-spaced WDM channels.

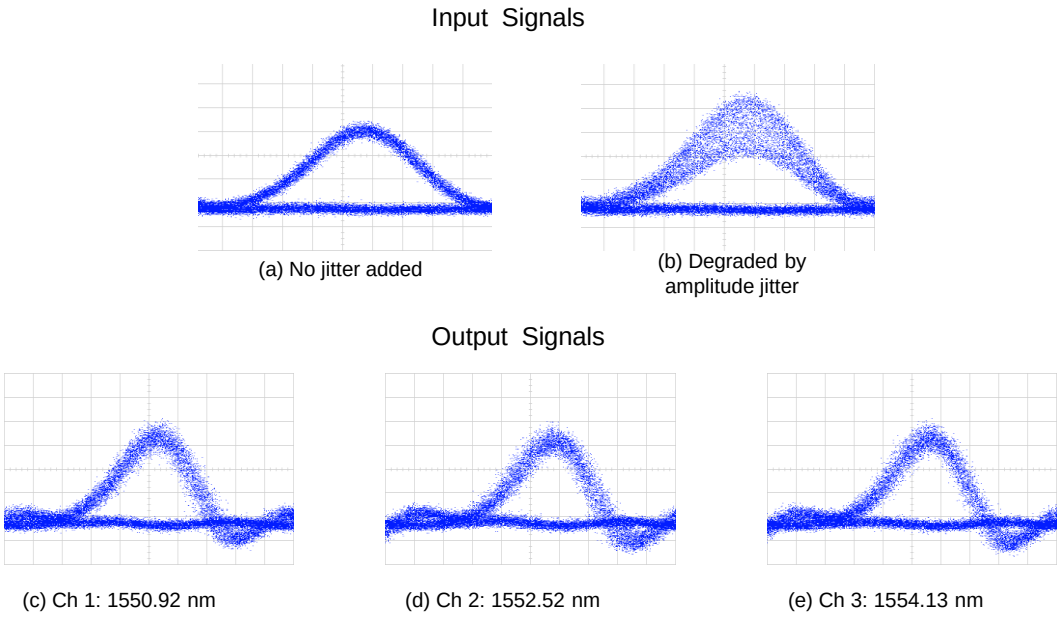

Fig. 3.6. Eye diagrams of RZ-OOK signals for 200-GHz spacing

Suppression of the amplitude jitter by our 2R regenerator can be seen for all three 200-GHz-spacied channels. The eye opening improvement is characterized by measuring the BER versus the receiver input power, as shown in Fig. 3.7. In the 200-GHz-spaced case, we observe a 3.0 dB improvement at BER level of 10^{-9} for 1550.92 nm, 3.1 dB improvement for 1552.52 nm and 3.0 dB improvement for

1554.13 nm. Overall, after regeneration, all three 200-GHz-spaced channels have a 3-dB improvement in BER measurements at 10^{-9} level.

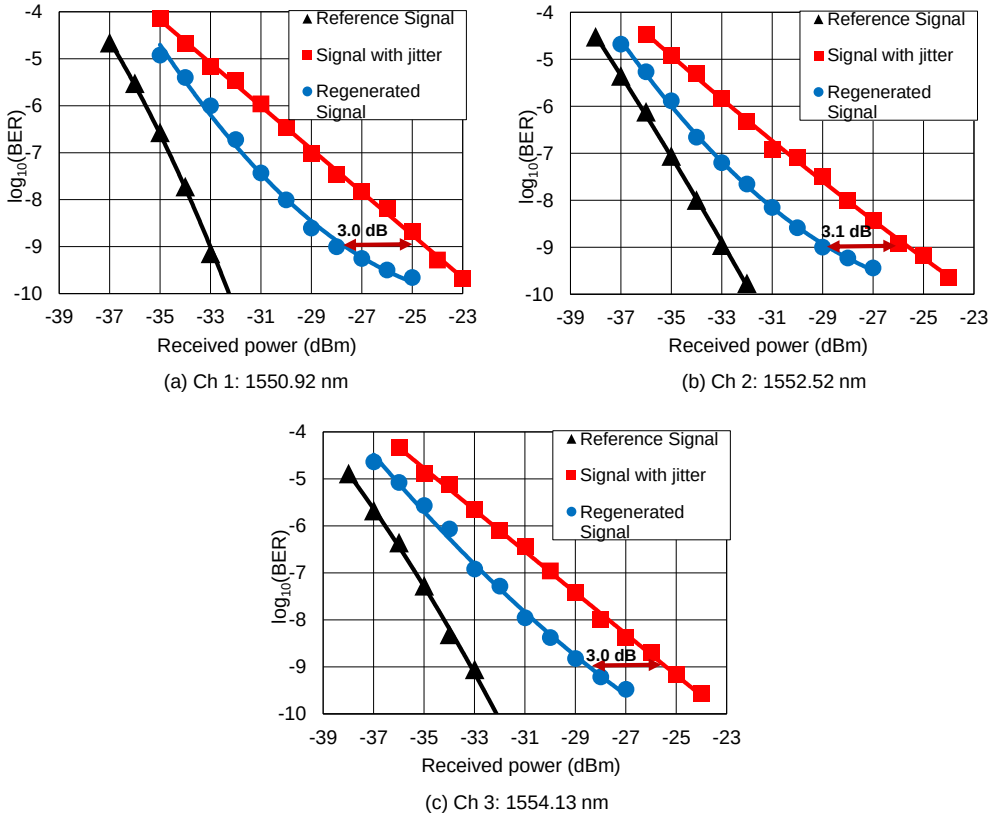

Fig. 3.7. BER vs. received power for 200-GHz spacing

3.2.4 100-GHz-Spaced Three-channel Results

Similar to the 200-GHz-spaced case, Figure 3.8 shows the eye diagrams of the regenerator input and output signals for regeneration experiment with 100-GHz spacing. Fig. 3.5 (a) illustrates the back-to-back signal not degraded by amplitude jitter while Fig. 3.5 (b) shows the input signal degraded by ±35% amplitude jitter. The regenerated output signal is shown in Figs. 3.8 (c)–(e) for three 100-GHz-

spaced WDM channels, whose wavelengths are 1551.72 nm, 1552.52 nm and 1553.33 nm.

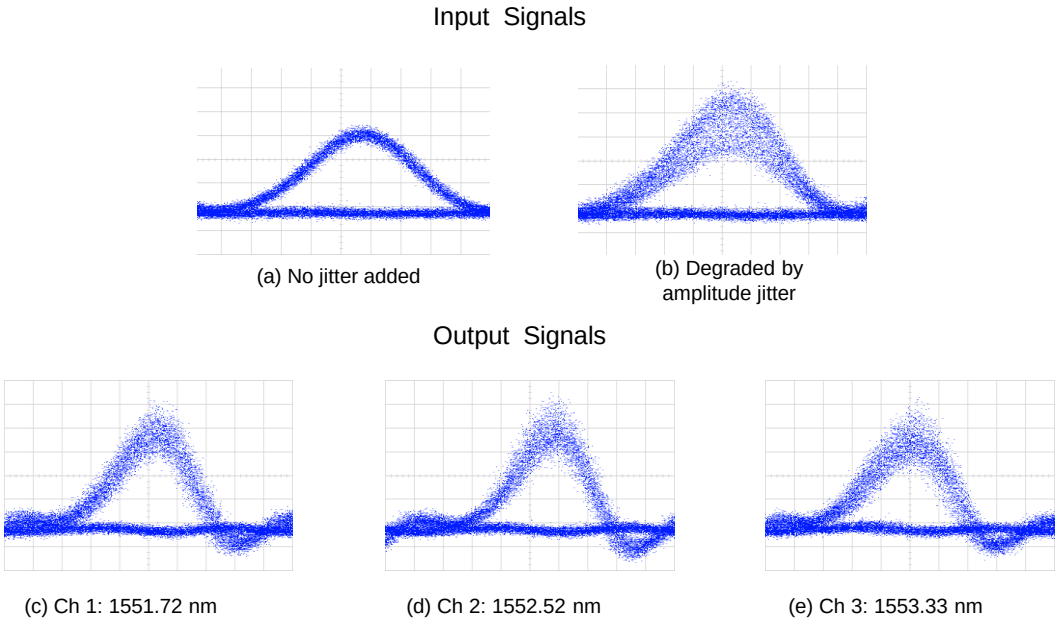

Fig. 3.8. Eye diagrams of RZ-OOK signals for 100-GHz spacing

Again, from the eye diagrams, we observe suppression of amplitude jitter for all three 100-GHz-spacied channels. This suppression is confirmed by the BER versus the receiver input power measurement, as shown in Figure 3.9. In the 100-GHz-spaced case, a 2.9-dB improvement is measured at BER level of 10^{-9} for 1551.72 nm, 2.1 dB improvement for 1552.52 nm and 2.7 dB improvement for 1553.33 nm. Overall, after regeneration, all three 100-GHz-spaced channels have more than 2-dB improvement in BER measurements at 10^{-9} level. This presents a clear evidence of the feasibility of 2R regeneration of 100-GHz-spaced channels in GDM-media-enabled Mamyshev 2R regenerator, proving that its performance is

not significantly degraded by the broadened spectrum of the neighboring channel. Overall, all three 200-GHz spaced channels show eye-opening improvement of more than 3 dB while all three 100-GHz spaced channels show eye-opening improvement of more than 2 dB, as shown in Fig.3.10.

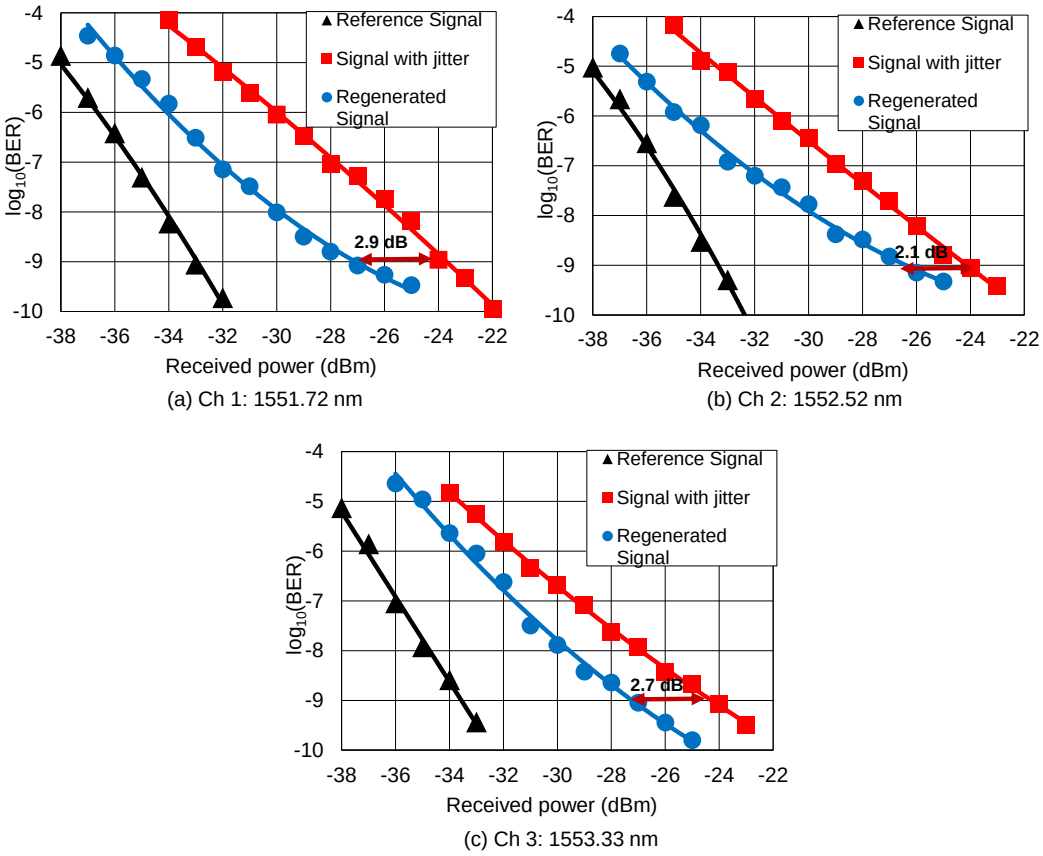

Fig. 3.9. BER vs. received power for 100-GHz spacing

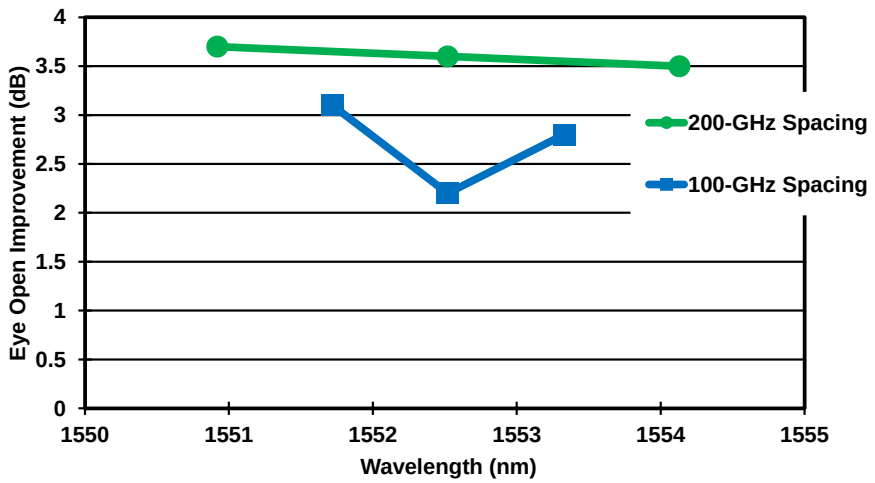

Fig. 3.10. Eye-opening improvements for each of the 3 channels, measured at BER of 10^{-9}.

3.3 Multi-Channel Optical Regeneration Experiment

3.3.1 GDM Nonlinear Medium for Multi-channel Regeneration

The GDM nonlinear medium is built of 5 complete and one partial (without PGDD) unit cells to have a better performance on multi-channel regeneration. As shown in Fig. 3.11, there are 5 identical 1-km-long sections of DCF (nonlinear constant γ = 5 $W^{-1}km^{-1}$) and one slightly longer 1.25-km DCF section close to the middle of the GDM, all separated by PGDDs. The dispersion of each PGDD is set to +130 ps/nm for 12 channels or to +150 ps/nm for 16 channels, so that the residual dispersion for each of 4 identical (1-km DCF + PGDD) unit cells is near +10 ps/nm or +30 ps/nm. The residual dispersion of the cell with a 1.25-km-long DCF is –20 ps/nm, which brings the accumulated residual dispersion back to zero halfway through the GDM. The last piece of 1-km-long DCF is left uncompensated, so that the total

GDM dispersion accumulated within each channel is only –100 ps/nm. Since more DCF and WDM combiners/splitters than previous three-channel case, the total loss of link increases to 35 dB. To compensate the big loss, eight RPUs are used to bi-directionally pump the GDM medium to transparency. Eight additional 1450/1550 nm pump/signal WDM combiners/splitters are inserted to make the Raman pump light bypass the lossy PGDDs.

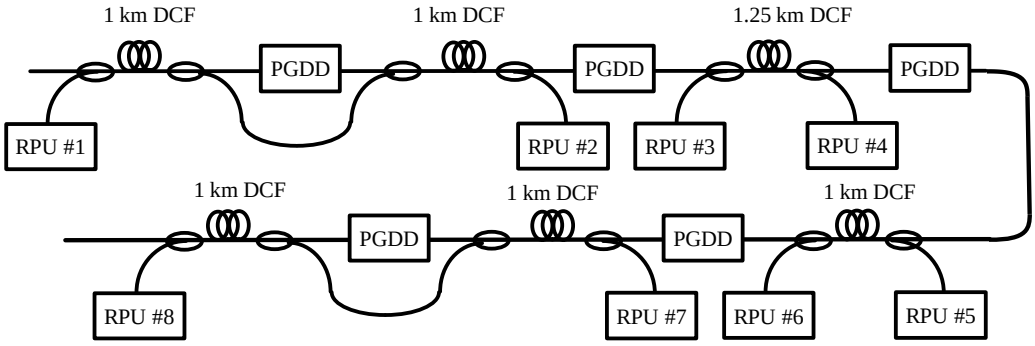

Fig. 3.11. GDM nonlinear medium for multi-channel regeneration

3.3.2 Multi-channel Experimental Setup

Experimental setup is shown in Figure 3.12, the 100-GHz-spaced 12-channel or 16-channel transmitter contains even ITU channel set and odd ITU channel set. All signals are first carved into 50% RZ pulses and OOK-modulated at 10.72 Gb/s by the same 2^{31}–1 pseudo-random bit sequence (PRBS) using two cascaded Mach–Zehnder modulators (MZMs). Another pair of independent MZMs impose a Nyquist-Johnson thermal noise generated by several cascaded RF amplifiers with 14-GHz bandwidths in order to emulate the real noise in transmission. Then a 2-km-long SMF is placed in the even-channel path to decorrelate the PRBS bit

patterns between the even and odd WDM channels. We also decorrelate the bit patterns within each of the even and odd channel sets by sending the combined signals through a 2.5-km-long DCF, yielding a 5-bit pattern delay between the adjacent channels of each 200-GHz-spaced set. The dispersion within each channel caused by the 2.5-km DCF is completely compensated by a preceding PGDD (set to +300 ps/nm) for 12-channel regeneration and 67% compensated by the PGDD (set to +200 ps/nm) for 16-channel regeneration, while the dispersion accumulated between the channels is preserved. It is important to note that the proper assessment of the inter-channel penalties in the regenerator demands averaging the performance over various initial bit delays between the neighboring channels [1, 45], which typically requires the use of two pattern generators (PGs) driven by independent clocks [4]. In lieu of the second PG, we decorrelate the clock frequencies of even and odd channels by introducing frequency modulation (FM) of the clock of a single PG. This is done by mixing the original 10.69 GHz sine-wave clock at a radio-frequency (RF) single sideband (SSB) modulator with a 30-MHz sine wave, FM-modulated with 50-kHz repetition frequency and ±100-kHz frequency deviation, which generates a 10.72-GHz clock with FM, as shown in Figure 3.9. The half-period of FM (10 μs) roughly corresponds to the delay of the even channels by the 2-km-long SMF and ensures that, after combining, even and odd channels have clocks whose frequency difference constantly changes in the range from –200 to +200 kHz, leading to continuous variation of the relative input

bit delays between the adjacent 100-GHz-spaced channels from − 0.64 to +0.64 bit periods over the span of 20-μs FM period.

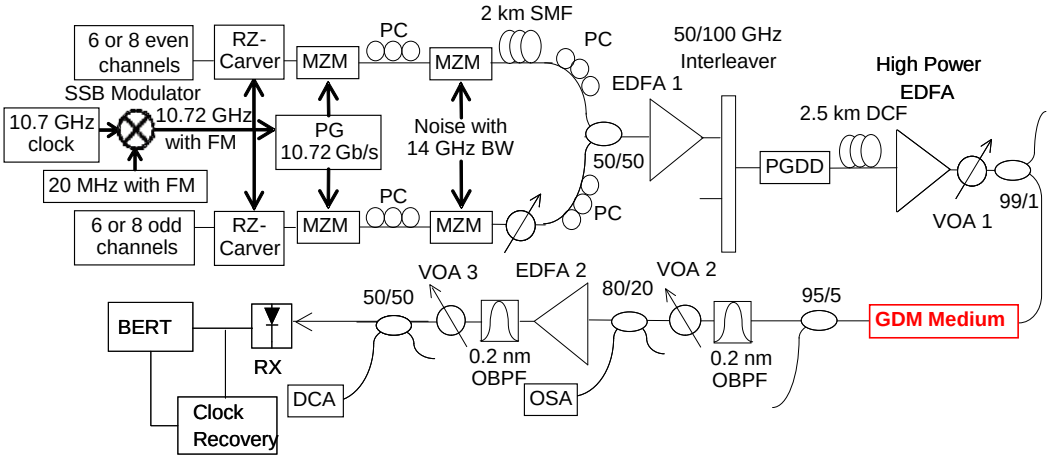

Figure 3.12. Experimental setup for multi-channel regeneration

All 12 or 16 WDM channels are set to be co-polarized, through polarization controllers, to ensure the worst case of inter-channel nonlinearities. After the first erbium-doped fiber amplifier (EDFA), a 50-to-100 GHz interleaver with 0.25-nm-wide passband is used to suppress the out-of-band amplified spontaneous emission (ASE) noise. After the second, high-power, EDFA the co-polarized signals enter Mamyshev regenerator consisting of the GDM medium that performs SPM-based spectral broadening and an optical bandpass filter (OBPF) selecting a frequency band offset by –0.05 nm (for 12 channels) or –0.07 nm (for 16 channels) from the original channel's center. In a real system, a simultaneous regeneration for all WDM channels can be done by using a comb filter such as an interleaver, but we use a single tunable 0.2-nm-wide OBPF because we only have one receiver. The

optimum total average power entering the GDM medium is 26 dBm (~33 mW/channel) in the 12-channel case and 27 dBm (~31 mW/channel) in the 16-channel case. The total average power at the output of the last 1-km DCF section falls to 22 dBm and 22.6 dBm for 12-channel and 16-channel regeneration, respectively, due to the Raman gain saturation. To make sure that the observed regeneration effect is not originating from the relatively slow saturation response of the Raman gain, we use the fast electronic noise fluctuations to produce the input amplitude jitter. At last, the output of the GDM-based regenerator is characterized by a pre-amplified direct-detection receiver.

3.3.3 12-channel Regeneration Results

The wavelength of 12 ITU channels are from 1549.32 nm to 1558.17 nm with 100-GHz spacing. In our experiments, due to the uneven gain ripple of RPUs for those channels, we have to use pre-emphasis technique to avoid ripple accumulation with increasing number of RPUs and optimize OSNR and Q-factor performance for all WDM channels [46]. Figure 3.13 shows the signal spectra for 12 channels at the input (blue) and output (red) of regenerator. A pre-emphasis technique has been used to enforce input and output of all 12 channels to be inverted versions of each other, indicating that all 12-channel signals have a relatively equal power at midway of transmission line to equalize OSNR and nonlinear phase shift among all the channels.

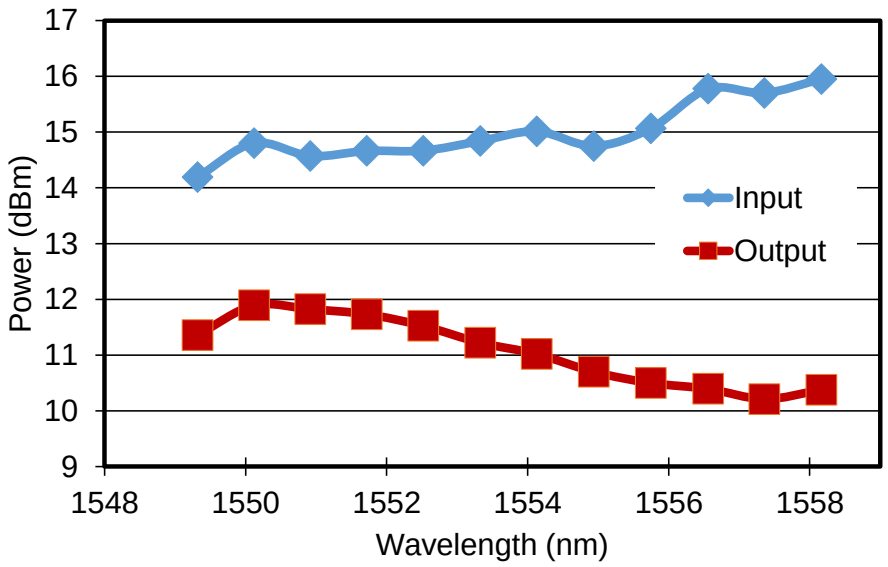

Fig. 3.13. Spectra ripple at input (blue) and output (red) among 12 channels

In the presence of distortion-like nonlinearity such as SPM, this technique ensures all WDM channels have equal SPM nonlinear phase shifts. Figure 3.14 (a) shows spectra with 0.016 nm resolution before (blue) and after (red) GDM nonlinear medium for all 12 channels. All of them have an equal amount of nonlinear phase shift and similar SPM-based spectral broadening. Figure 3.14 (b) gives a zoom-in view on spectrum of channel #8 and shows a significant spectral broadening.

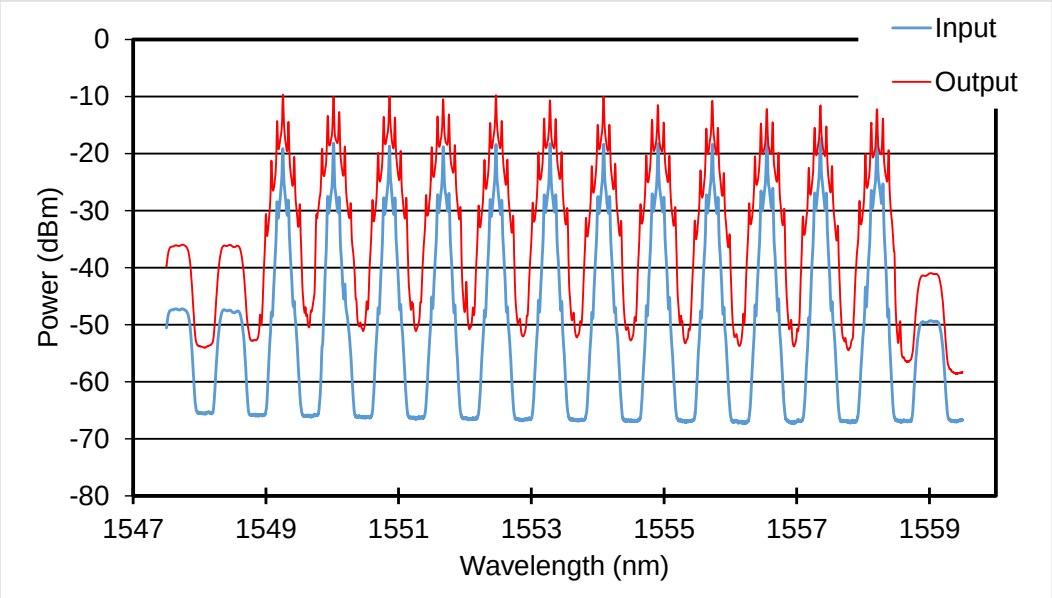

(a)

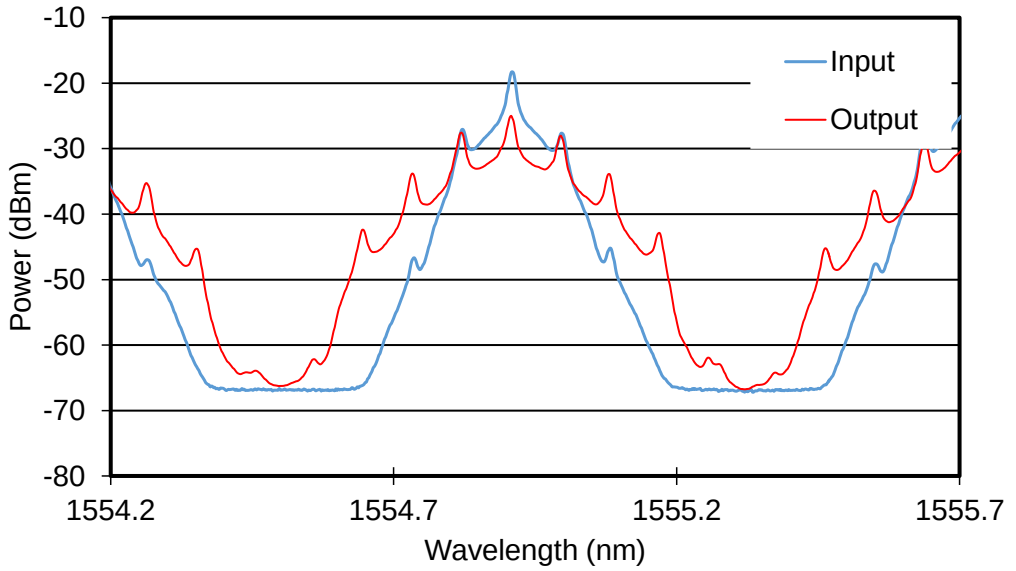

(b)

Fig. 3.14. Spectrum with 0.016 nm resolution before (blue) and after (red) GDM nonlinear medium: (a) 12 channels; (b) channel #8.

Figure 3.15 shows the eye-diagrams of degraded input signal (±35% amplitude jitter) and regenerated output signal for all 12 channels for optimum value of –0.05 nm detuning of tunable filter from the input signal's center wavelength. For all 12 channels we can see that the regenerated output pulse has a much cleaner amplitude compared to the input pulse.

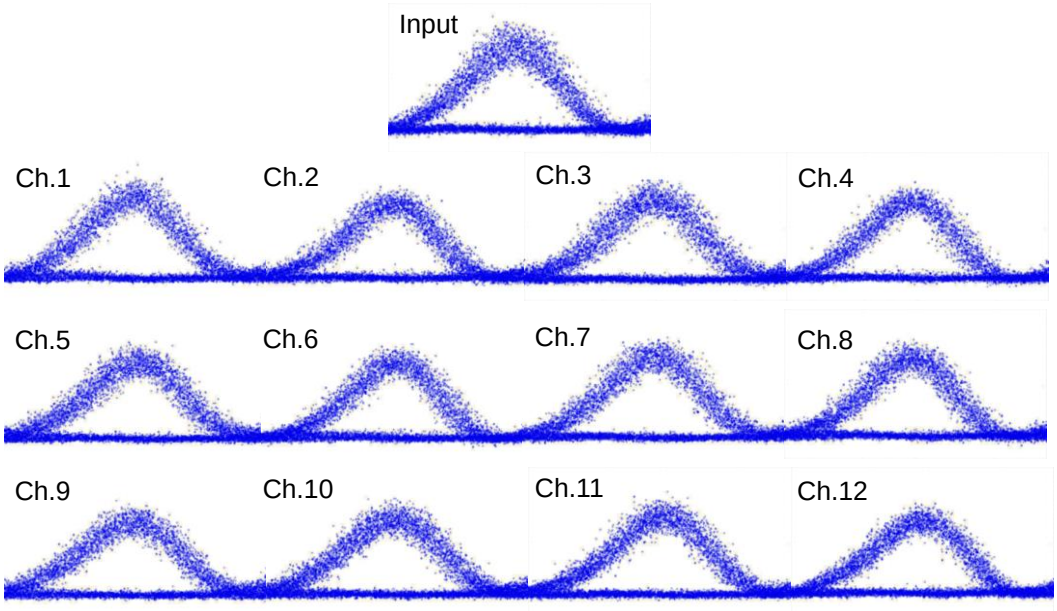

Fig. 3.15. Eye diagrams of noise-degraded input and regenerated output signals

The BER curves measurements are implemented to quantify the eye opening improvement. The bit error rates (BERs) vs the receiver input power are summarized for all channels in Fig. 3.16. Owing to large amount of the loaded broadband noise, the degraded signal hits a noise floor above BER of 10^{-9}, but the regenerated signal reaches below 10^{-9}. Thus, to quantify the regeneration performance, Figure 3.17 presents the eye-opening improvement not at 10^{-9}

(infinite) but at 10^{-8} BER level (more conservative estimate). This eye-opening improvement in Fig. 3.17 has a minimum of 3 dB for all 12 channels.

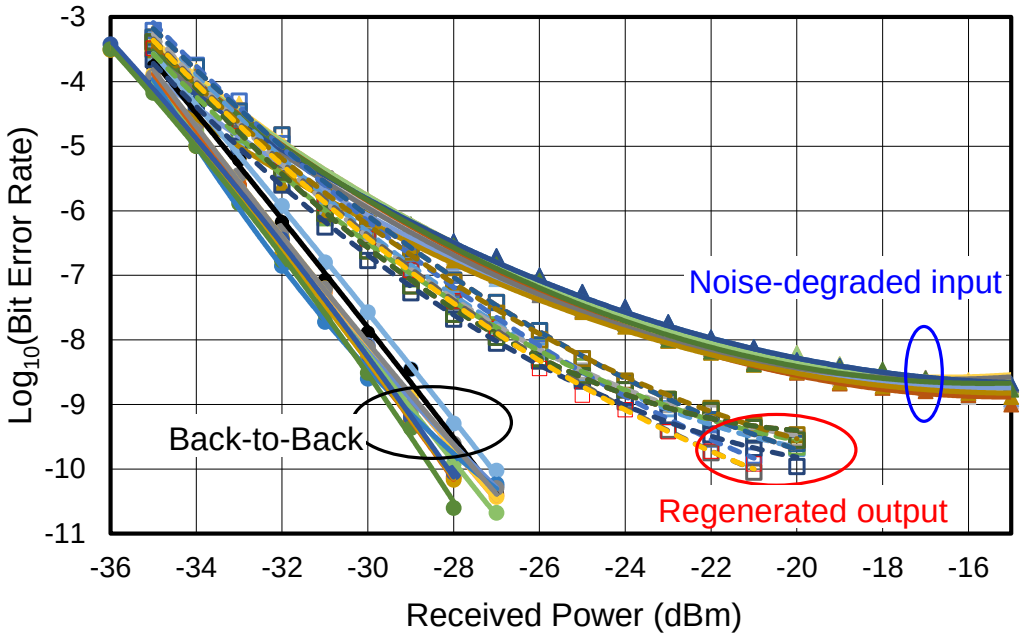

Fig. 3.16. BER vs received power for all 12 channels: solid triangles – degraded input; empty squares – regenerated output; solid circles – back to back

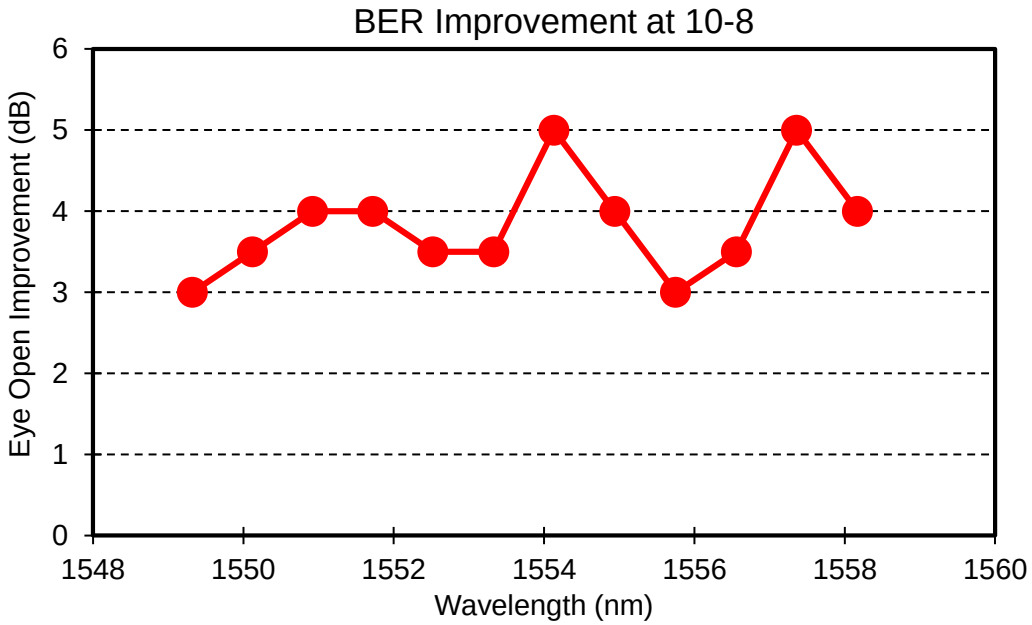

Fig. 3.17. Eye opening improvements measured for all 12 channels

3.3.4 16-channel Regeneration Results

The wavelengths of 16 ITU channels are from 1543.73 nm to 1555.75 nm with 100-GHz spacing. Figure 3.18 shows the signal powers for 16 channels at the input (blue) and output (red) of regenerator. A pre-emphasis technique has also been used to enforce input and output power ripples of all 16 channels to be inverted versions of each other to optimize OSNR and nonlinear phase shift among all the channels.

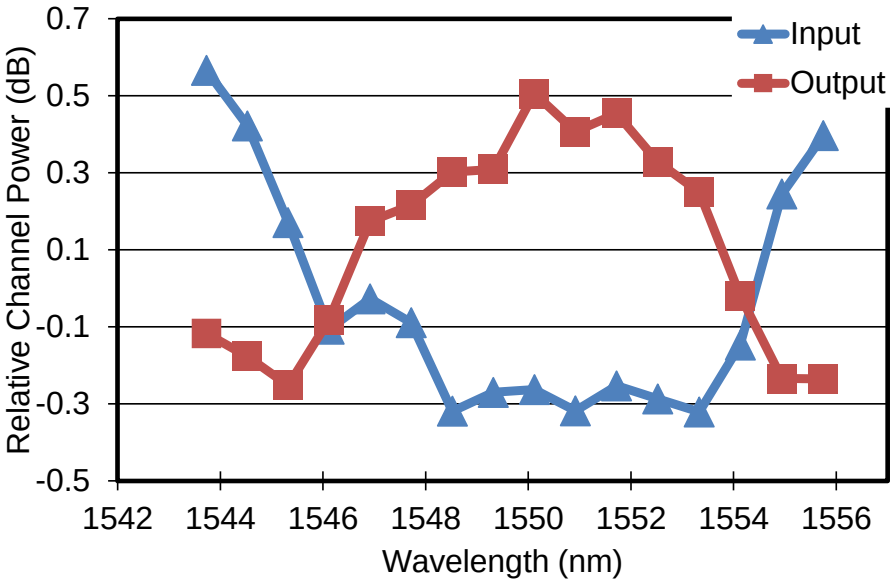

Fig. 3.18. Power ripple at input (blue) and output (red) among 12 channels

Fig. 3.19 (a) shows spectra with 0.016 nm resolution before (blue) and after (red) GDM nonlinear medium for all 16 channels. All of them have an equal amount of nonlinear phase shift and similar SPM-based spectral broadening. Fig. 3.19 (b) shows more detailed spectra of four representative channels and each of them shows a similar and significant spectral broadening.

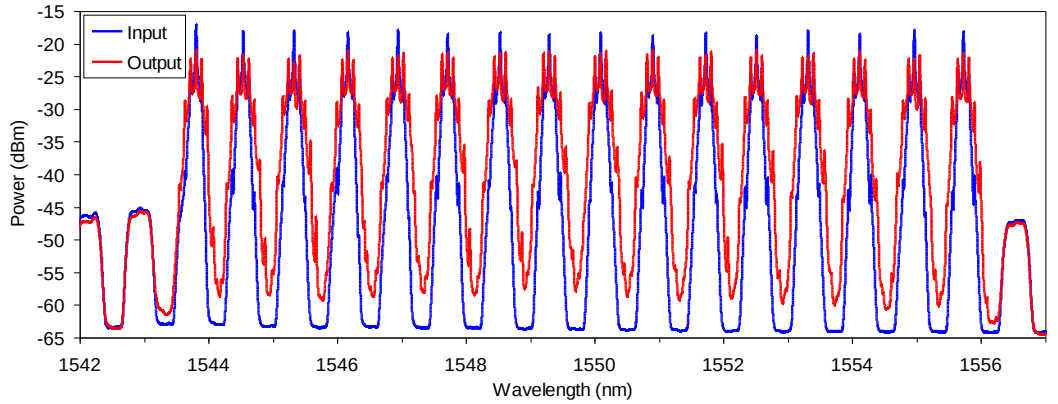

(a)

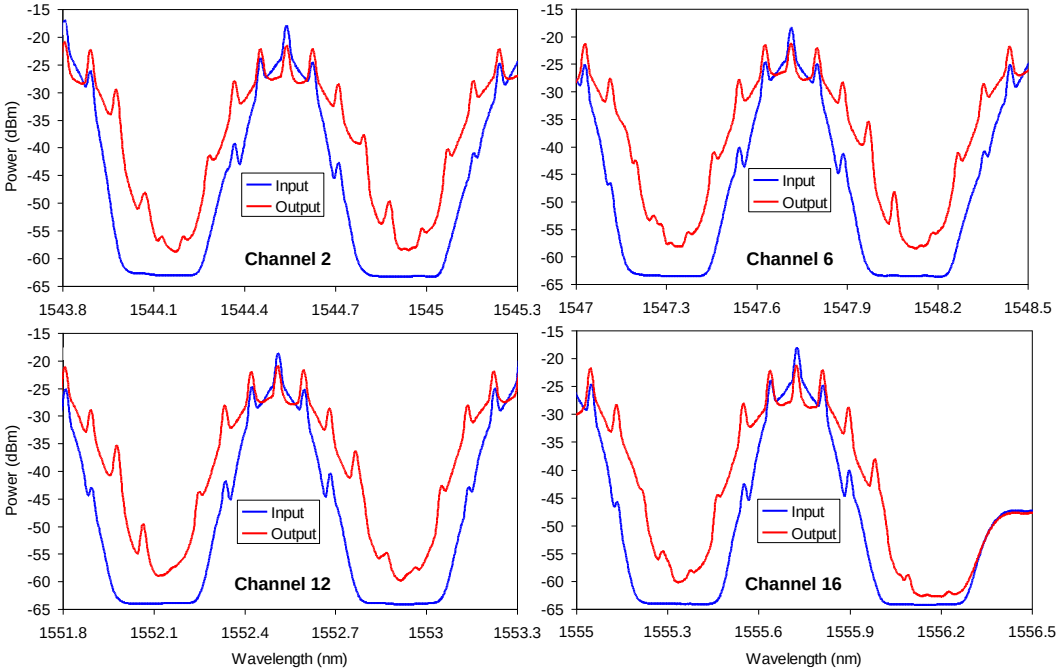

(b)

Fig. 3.19. Spectrum with 0.016 nm resolution before (blue) and after (red) GDM nonlinear medium: (a) 16 channels; (b) channel #2, #6, #12 and #16.

Fig. 3.20 (a) shows the eye-diagrams of degraded input signal (±35% amplitude jitter) and regenerated output signal for all 16 for optimum value of –0.07 nm detuning of tunable filter from the input signal's center wavelength. For all 16 channels we can see that the regenerated output pulse much has a much cleaner amplitude compared to the input pulse. Figures 3.20 (b) and (c) show 5-bit and 10-bit patterns before and after regeneration for 1555.75-nm channel.

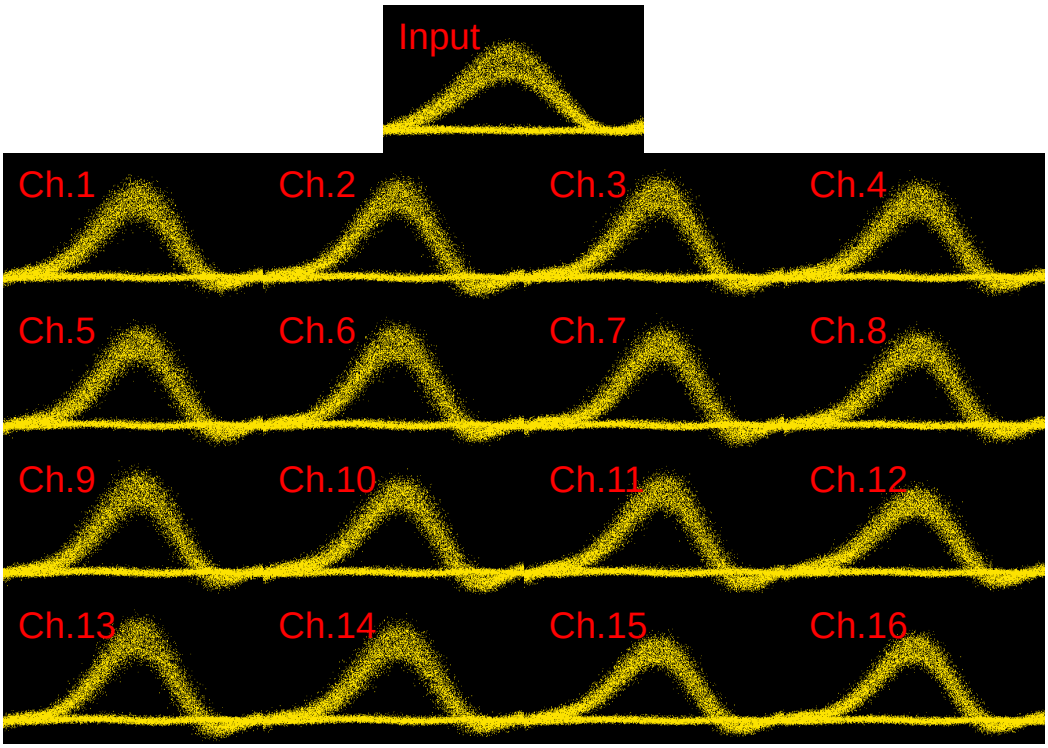

(a)

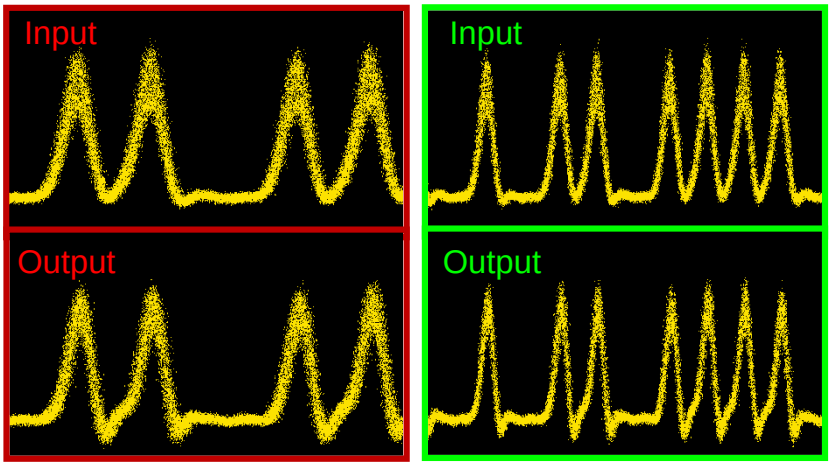

(b) (c)

Fig. 3.20. Eye diagrams of noise-degraded input and regenerated output signals:
(a) 16 channels; (b) 5-bit pattern (1555.75-nm channel);
(c) 10-bit pattern (1555.75-nm channel)

The BER measurements are implemented to quantify the eye-opening improvement. The BERs vs the receiver input power curves are summarized for all 16 channels in Fig. 3.21. To quantify regeneration performance, Fig. 3.22 presents the eye-opening improvement at 10^{-9} BER level. This eye-opening improvement in Figs. 3.21, 3.22 has a minimum value of 5 dB for all 16 channels.

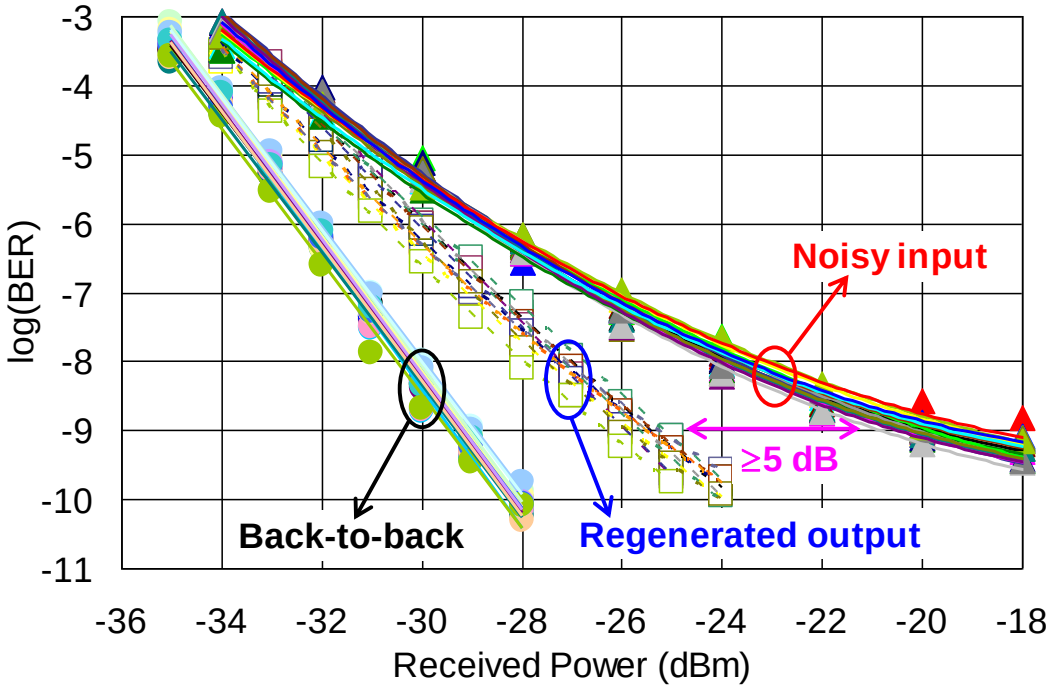

Fig. 3.21. BER vs received power for all 16 channels: solid triangles – degraded input; empty squares – regenerated output; solid circles – back to back

To summarize, in this chapter, we built a novel GDM nonlinear medium that can enable the WDM operation in any SPM-based 2R regenerator. We use the GMD medium in Mamyshev regenerator to adapt it to WDM operation. Then, we experimentally demonstrate the simultaneous 2R regeneration of 3, 12 and 16

WDM channels with 100 GHz spacing in a stand-alone Mamyshev regenerator based on the GDM nonlinear medium. The results show that neither increased number of channels nor narrow channel spacing degrades the performance of our multi-channel regenerator.

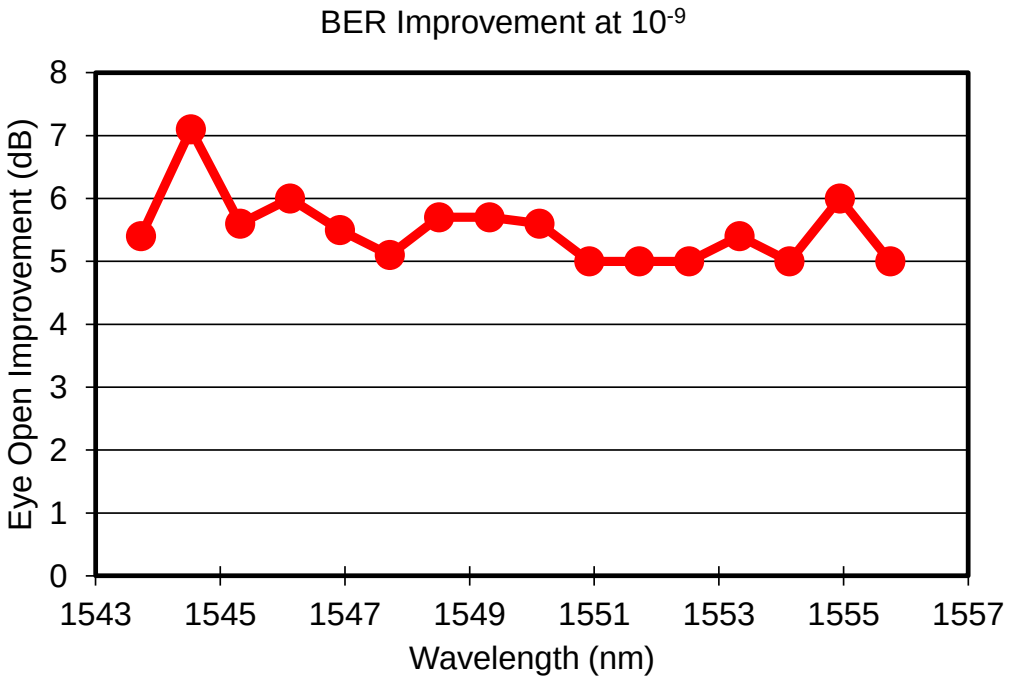

Fig. 3.22. Eye opening improvements measured for all 16 channels

CHAPTER 4

A PHASE-PRESERVING AMPLITUDE REGENERATOR BASED ON NOLM

Compared to traditional on-off keying amplitude modulation, signals using phase encoding, e.g., return-to-zero differential phase-shift keying (RZ-DPSK), are preferable in communication systems due to their robustness to nonlinear effects, improved dispersion tolerance, and high spectral efficiency. Nevertheless, DPSK formatted signals still suffer amplitude jitter caused by intrachannel four-wave mixing, as well as from and amplitude noise conversion to phase noise, known as the Gordon–Mollenauer effect [47], which is the major impairment in phase-encoded systems. One easy and simple way to deal with it is to employ phase-preserving amplitude regeneration. In this chapter, we demonstrate the phase-preserving amplitude regeneration of useful 50%-duty-cycle RZ-DPSK signals by using a NOLM.

4.1. NOLM-based Regenerator Setup

The setup of our NOLM-based regenerator is shown in Fig. 4.1. It consists of a 95:5 coupler, a piece of nonlinear fiber (5.1 km of non-zero dispersion-shifted fiber, or NZDSF, with dispersion D = 4 ps/nm/km, nonlinearity γ = 1.5 $W^{-1}km^{-1}$, and attenuation α = 0.2 dB km^{-1}), and a DA implemented by an isolator (37 dB isolation) instead of directional amplifiers. We call this regenerator as DA-NOLM regenerator. In addition, there are two polarization controllers inside and outside

the loop to adjust the linear phase bias, in order to adapt it to working with high-duty-circle pulses, as we discussed in chapter 2.

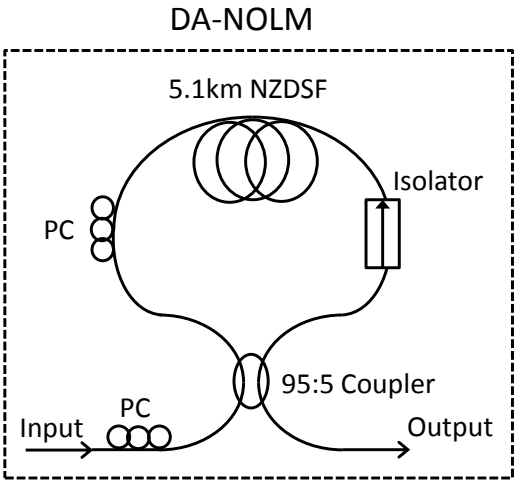

Fig. 4.1. Schematic diagram of DA-NOLM

The input signal is separated into two unequal counter-propagating beams by 95:5 coupler. The weaker beam propagates through the isolator in forward direction, experiencing only a small insertion loss. Because of its weak strength, signal has negligible SPM phase shift during its propagation through NZDSF. The stronger beam passes through NZDSF first and gains a relatively large nonlinear phase shift. Then it is greatly attenuated by the isolator (37 dB in our case). The stronger beam has lower power than the weaker beam when they encounter at coupler. The low-power beam (the original "stronger beam") with input-power-dependent phase shift and a higher-power beam (originally, "weaker beam") with almost unperturbed phase interfere at the NOLM output. The output signal's amplitude is thus determined by the interference between the counter-propagating beams while the

output phase is dominated by the high-power beam with unperturbed phase. This characteristic leads to nonlinear power and phase transfer curves, where a plateau can be found in both power and phase curves to achieve amplitude regeneration without disturbing the phase.

4.2 Phase-Preserving Amplitude Regeneration Experiment

4.2.1 Experiment Setup

Fig. 4.2 illustrates the experimental setup for phase-preserving amplitude regeneration using DA-NOLM. The transmitter has only one wavelength of 1546 nm from a DFB laser. The signal is DPSK-modulated at 10.7 Gb/s by a 2^{31}–1 pseudo-random bit sequence (PRBS) pattern and then carved into 50% RZ pulses. The VOA 1 is placed in front of EDFA1 to adjust loaded ASE noise by varying attenuation. An OBPF is used to filter out out-of-band noise before launching into the high-power EDFA. The average input power into DA-NOLM regenerator is adjusted by controlling the second VOA2 in order to achieve the optimum regeneration. The resulting signal can either bypasses the DA-NOLM or go through it for regeneration. VOA3 controls the power into the receiver consisting of a pre-amplifier EDFA2, OBPF, delay interferometer (DI), and a balanced photodetector.

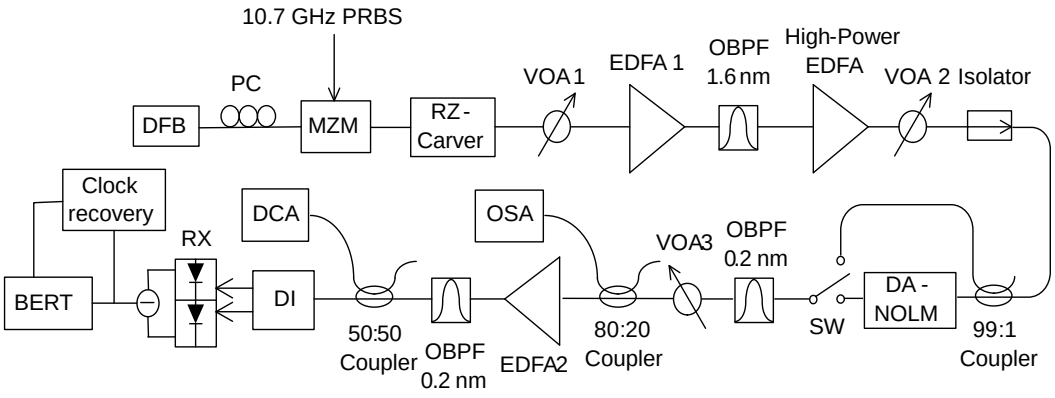

Fig. 4.2. Experimental setup for DA-NOLM regeneration

4.2.2 Experiment Results

To study the performance of DA-NOLM regenerator, we implement the experiment with two different type of noise, namely the amplitude jitter and ASE noise. First, only amplitude jitter with ±30% fluctuation is introduced by shifting the bias voltage of Mach-Zehnder modulator (MZM) from the optimum for DPSK modulation. The average input power of DA-NOLM regenerator is set to 24 dBm for optimized regeneration. The optical signal-to-noise ratio (OSNR) in 0.1 nm spectral bandwidth is now set to 27.5 dB for the signal launched into the DA-NOLM. The eye diagrams of the input signals before and after the DPSK demodulation are shown in Fig. 4.3 (a) and (b) while output signals shown in Fig 4.3 (b) and (d). As we can see, the eye diagram shows a significant suppression on amplitude jitter after regeneration in Fig 4.3 (b), compared to the input in Fig. 4.3 (a).

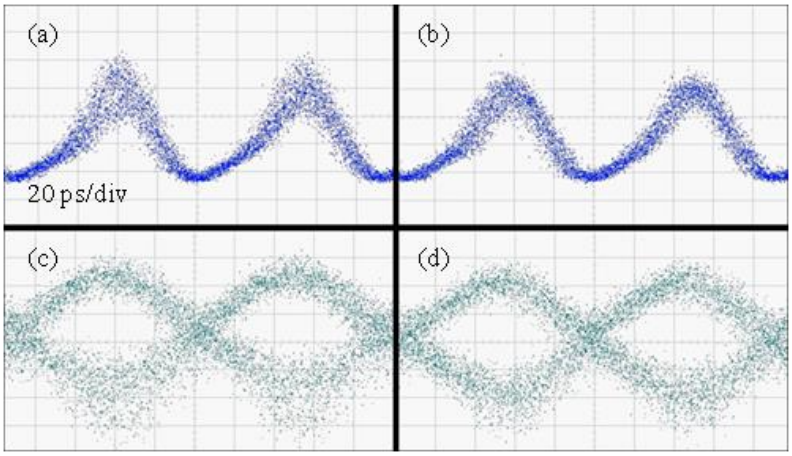

Fig. 4.3. Eye diagrams for amplitude-jitter-only case: (a) input before demodulation; (b) output before demodulation; (c) input after demodulation; (d) output after demodulation

The eye opening improvement between the signals at the input and output of DA-NOLM is characterized by measuring the BER versus the receiver input power, as shown in Fig. 4.4. The reference signal has the same OSNR of 27.5 dB, but without the amplitude jitter, measured after bypassing the NOLM. This jitter reduction in eye diagrams is confirmed by a 2 dB eye-opening improvement observed in BER measurements at 10^{-9} BER level.

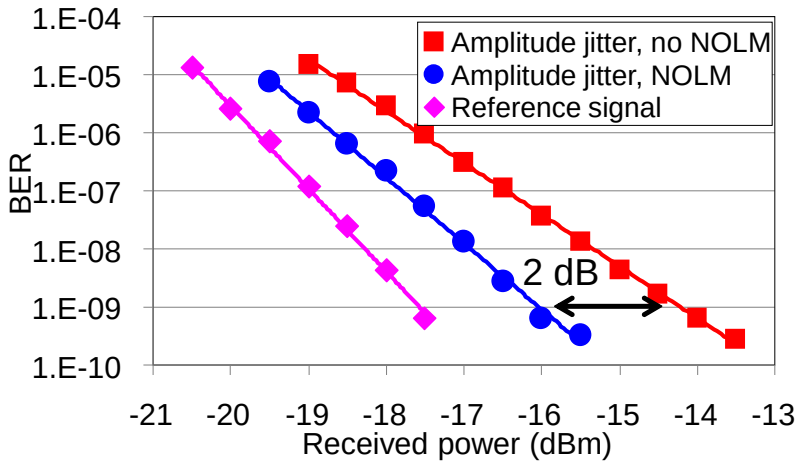

Fig. 4.4. BER vs. receiver power for amplitude-jitter-only case

Then, we use the same amplitude-impaired signal but add more ASE noise to signal by adjusting VOA1. The 0.1-nm OSNR of the signal launched into the DA-NOLM is reduced to 20 dB. The eye diagrams and BER versus the receiver input power curves are shown in Figures 4.5 and 4.6, respectively. Again, we see a considerable eye improvement by the DA-NOLM, quantified to be 1.5 dB in BER measurements at 10^{-9} level. The 0.5-dB lower improvement figure compared to the amplitude-jitter-only case may have come from two factors: a) out-of-band ASE, not cleaned out adequately due to relatively wide 1.6-nm bandwidth of the OBPF after EDFA1, couples to and degrades the signal during nonlinear propagation in NOLM; b) the range of the fluctuations produced by the combination of the amplitude jitter and ASE might be wider than the regenerator's acceptance range.

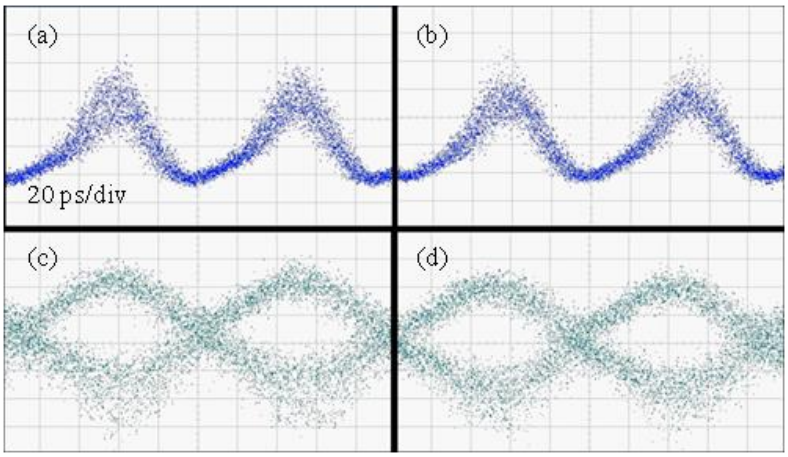

Fig. 4.5. Eye diagrams for ASE-degraded case: (a) input before demodulation; (b) output before demodulation; (c) input after demodulation; (d) output after demodulation

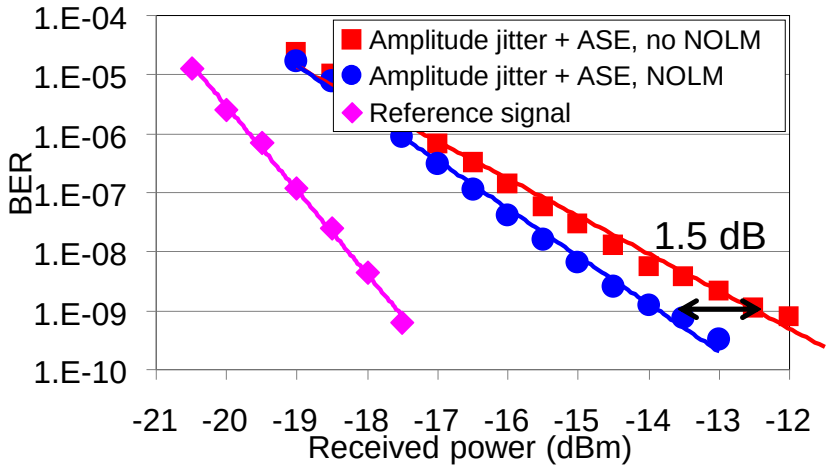

Fig. 4.6. BER vs. receiver power for ASE-degraded case

4.3 Amplitude-to-Phase Noise Prevention Experiments using NOLM regenerators

4.3.1 Experimental Setup

The experimental setup for study of nonlinear phase suppression by using DA-NOLM is shown in Fig. 4.7. The 1546-nm light from a DFB laser is DPSK-modulated at 10.7 Gb/s by a 2^{31}-1 pseudo-random bit sequence (PRBS) pattern and then carved into 50% RZ pulses. The signal is loaded with ASE noise by varying VOA1 before launching into EDFA1. After the high-power EDFA, the average input power to DA-NOLM is adjusted by VOA2 for optimized regeneration. The input signal either bypasses the NOLM or goes through it for regeneration by switch SW1. A piece of 40 km NZDSF is placed after EDFA2 and is used to translate amplitude noise into phase noise by the Gordon-Mollenauer effect. This fiber can be also bypassed through switches SW2 and SW3. VOA3 controls the power into the receiver consisting of a pre-amplifier EDFA3, optical bandpass filter (OBPF), delay interferometer (DI), and a balanced photodetector.

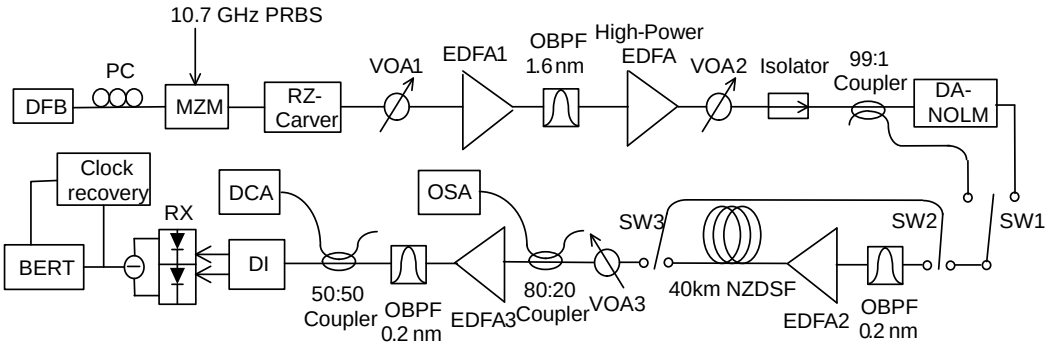

Fig. 4.7. Experimental setup for nonlinear phase prevention

Again, two different types of noise are used to study the regeneration performance in the experiment. First, we only introduce ±40% amplitude jitter by shifting the bias voltage of Mach-Zehnder modulator (MZM) from the optimum for DPSK modulation. The average input power of NOLM for maximum regeneration is set to 24 dBm for optimized regeneration. By adjusting VOA1, the optical signal-to-noise ratio (OSNR) in 0.1 nm spectral bandwidth is set to 27.5 dB for the signal launched into the NOLM. The output power of EDFA2 is set to P_2 = 11.4 dBm to accumulate noticeable nonlinear phase shift of ~0.75 rad in a piece of 40 km NZDSF (effective nonlinear length L_{eff} =18 km).

4.3.2 Experimental Results

The eye diagrams of the signals with and without passing through NOLM both before and after the DPSK demodulation are shown in Fig. 4.8. As we can see, the eye diagram shows a significant suppression on amplitude jitter after regeneration in Fig. 4.8 (b), comparing with input in Fig. 4.8 (a). This jitter reduction is also seen in the demodulated DPSK eye diagram.

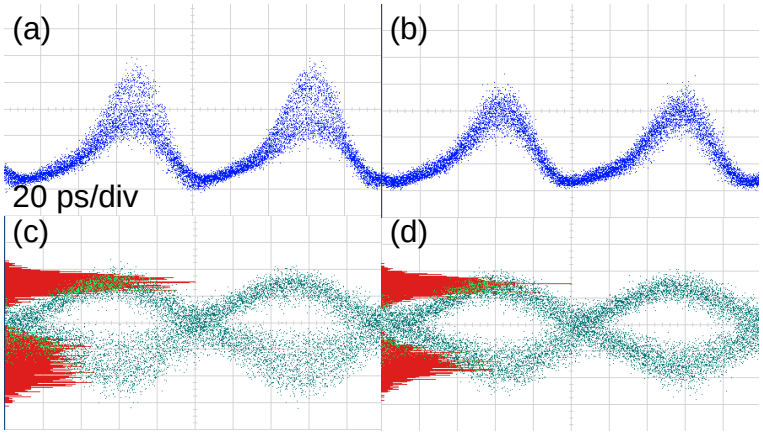

Fig. 4.8. Eye diagrams for amplitude-jitter-only case: (a) input before demodulation; (b) output before demodulation; (c) input after demodulation; (d) output after demodulation

The histograms of the demodulated eye diagram are given as well in Fig. 4.8 (red part). They confirm the lack of additional phase jitter due to phase-preserving amplitude regeneration by DA-NOLM. The eye opening improvement between the signals with and without passing through NOLM is characterized by measuring the BER versus the receiver input power after 40 km transmission, as shown in Fig. 4.9, where a 2 dB improvement is observed at 10^{-9} BER level. Compared to the eye opening improvement before the NZDSF, the eye opening improvement after the NZDSF is larger, owing to the reduction of the nonlinear phase noise, in addition to the amplitude jitter, in the DA-NOLM-assisted case.

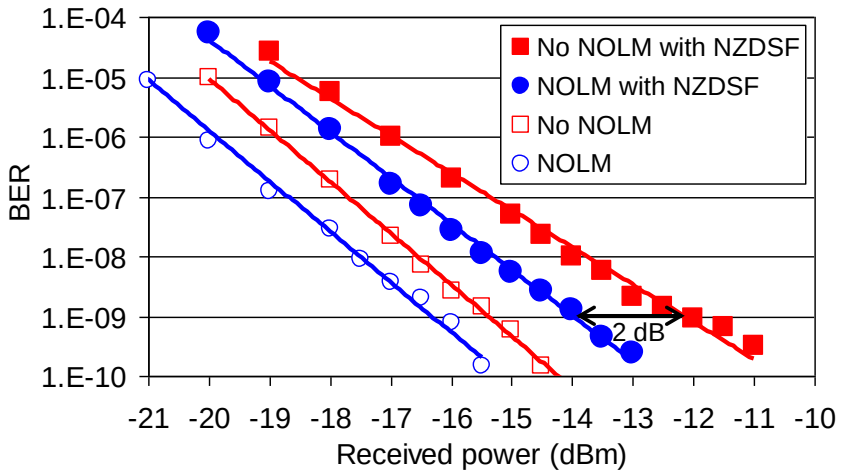

Fig. 4.9. BER vs. receiver power for amplitude-jitter-only case

Then, we turn off amplitude jitter but add more ASE noise to signal by adjusting VOA1. The 0.1-nm OSNR of the signal launched into the DA-NOLM is reduced to 17.3 dB. The eye diagrams and BER versus the receiver input power curves are shown in Fig. 4.10 and Fig. 4.11, respectively. Again, we see a considerable eye improvement by the DA-NOLM, quantified to be 1.5 dB in BER measurements at 10^{-9} level.

To summarize this chapter, we experimentally demonstrate amplitude regeneration of 50% duty-cycle RZ-DPSK signal by using a NOLM. An eye-opening improvement of 1.5 dB is observed for a signal degraded by a combination of ASE noise and amplitude jitter. Further, we employ the NOLM regenerator before a 40-km-long transmission link and show that it prevents amplitude-to-phase noise conversion (Gordon-Mollenauer effect), resulting in a 2-dB eye-opening improvement.

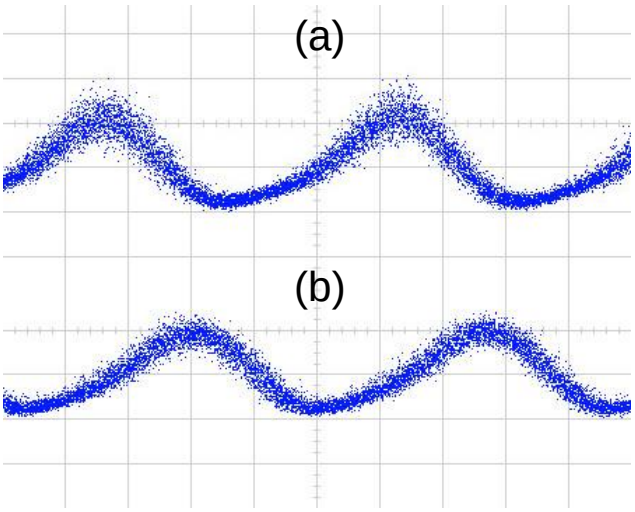

Fig. 4.10. Eye diagrams for ASE-only case: (a) ASE-degraded signal; (b) regenerated signal.

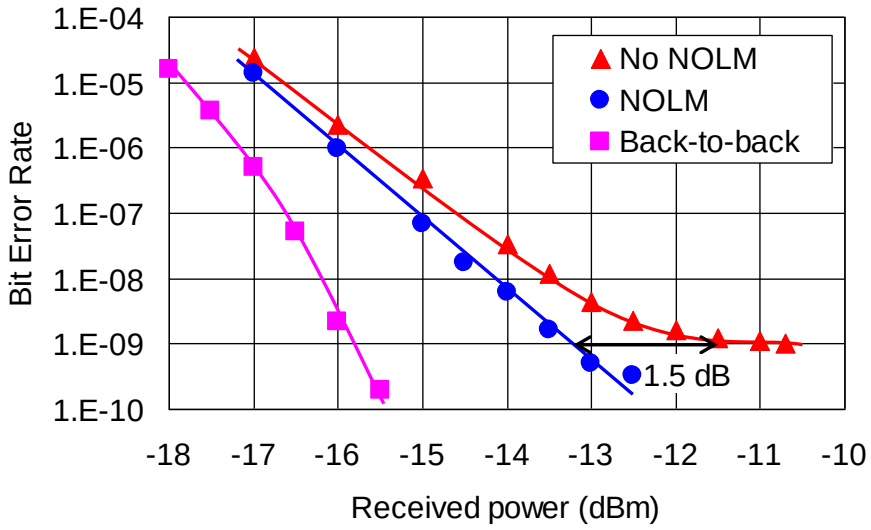

Fig. 4.11. BER vs. receiver power for ASE-only case

CHAPTER 5

ALL-OPTICAL REGENERATION SCHEME FOR 16-QAM SIGNALS

With increasing demand for higher transmission capacity and bit rates, the combination of amplitude and phase modulation in multilevel encoding, known as quadrature amplitude modulation (QAM), has come into focus of the optical communication research. QAM leads to higher spectral efficiency and transmission capacity in WDM systems, but also results in a higher sensitivity to amplitude and phase noise [48]. Therefore, with the growing popularity of multi-level QAM formats, there is need for 2R regenerations of the accumulated linear noises (e.g. ASE) as well as of the nonlinear phase noise converted from amplitude noise due to Gordon-Mollenauer effect [47].

The difficulty of 16-QAM regeneration is in doing multi-level regeneration on both amplitude and phase. Recently, regeneration using phase-sensitive amplifiers (PSAs) become very popular because of PSA's phase squeezing capacity. Several PSA-based phase regenerators of some phase-encoded modulation formats have been recently demonstrated [49–52]. PSA-based regenerators can be operated in saturated regime to achieve simultaneously amplitude and phase regeneration [53]. Unfortunately, saturated PSAs cannot work with any multi-level amplitude regeneration. Overall, the problem of regenerating the most popular 16-QAM format is still open. In this chapter, we propose a novel scheme for 16-QAM signal regeneration based on PSAs and numerically investigate performance of this

scheme using constellation analysis. Unlike the saturated PSA scheme, our scheme is potentially compatible with multi-channel operation, if the HNLF is replaced by the GDM medium.

5.1 Introduction to novel 2R Regenerator

First, we introduce a new kind of amplitude regenerator using a PSA and a piece of HNLF, shown in Fig. 5.1 (top). The operation principle is to use quadrature squeezing of PSAs and SPM-induced nonlinear phase shift. Let us assume a signal with only amplitude fluctuation on X quadrature. During its propagation in the HNLF, the signal acquires a nonlinear phase shift due to self-phase modulation. So does the amplitude fluctuation. By carefully controlling the phase shift, the noise on X quadrature is converted to the noise on Y quadrature, so that the noise on Y quadrature can be suppressed through squeezing of Y quadrature by a following PSA, to obtain an amplitude-regenerated signal at output. This regenerating process is shown in Fig. 5.2 (bottom).

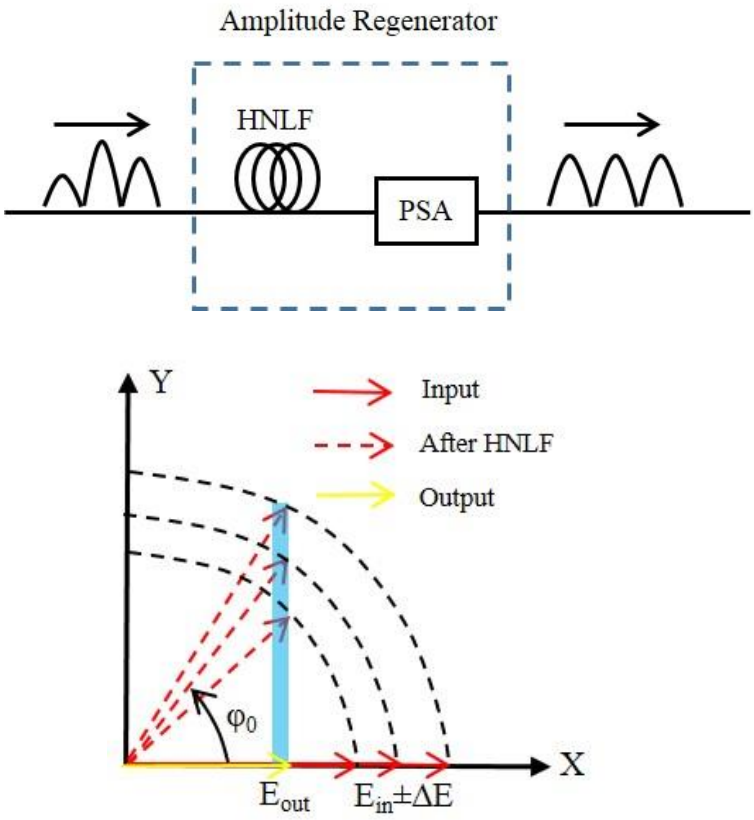

Fig. 5.1. Block diagram of 16-QAM signal regeneration scheme (top) and polar plot of amplitude regeneration (bottom).

Considering an input signal E_{in}, it only has amplitude A_0 and fluctuation ΔA_0 on X quadrature and no Y quadrature component. Then the signal goes through a piece of HNLF, whose nonlinear coefficient and fiber length are γ and L. The nonlinear phase shift introduced by self-phase modulation can be given by

$$\varphi \approx \gamma L(A_0^2 \pm 2A_0\Delta A_0). \tag{5.1}$$

At the end of the fiber, the complex form of signal with noise is given by

$$E_1 = (A_0 \pm \Delta A_0)\exp(i\varphi). \tag{5.2}$$

Here we define a parameter $\varepsilon=\Delta A_0/A_0$, describing the ratio of noise to signal for amplitude. Then equation (5.2) becomes

$$E_1 = A_0(1\pm\varepsilon)\exp[i\varphi_0(1\pm 2\varepsilon)], \tag{5.3}$$

where $\varphi_0=\gamma L A_0$ is the nonlinear phase shift for the signal without noise. When the signal is amplified by a PSA, only X quadrature is preserved, whose form is

$$X_1 = A_0(1\pm\varepsilon)\cos[i\varphi_0(1\pm 2\varepsilon)]. \tag{5.4}$$

Finally, the expression of normalized amplitude fluctuation is given by

$$\frac{\Delta X_1}{X_1} = \frac{\Delta X_1 - X_1}{X_1} = (1\pm\varepsilon)\frac{\cos[i\varphi_0(1\pm 2\varepsilon)]}{\cos(i\varphi_0)} - 1. \tag{5.5}$$

Compared to the input signal, the amplitude fluctuation of output signal can be reduced by adjusting nonlinear phase shift φ_0 through equation (5.5). Theoretically, we can find the optimal value of φ_0 to minimize the value of equation (5.5) for any jitter ε. Fig. 5.2 is numerical solution of equation (5.5). For different amplitude jitter, the optimum phase shift should be slightly adjusted to achieve the maximum regeneration.

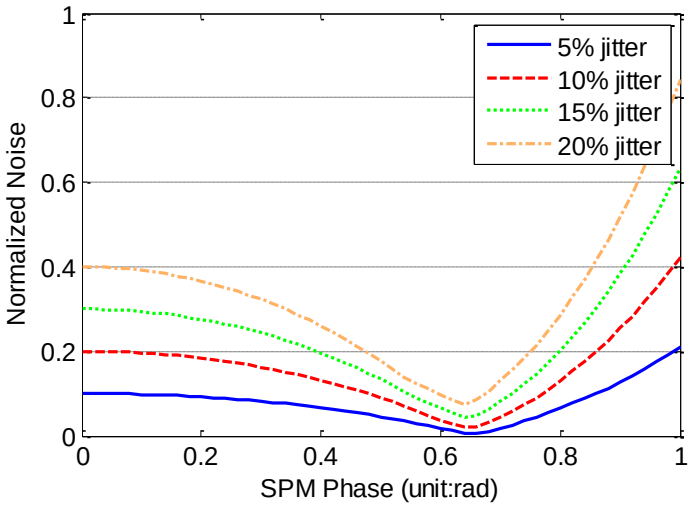

Fig. 5.2. Normalized noise versus SPM phase shift

5.2 16-QAM Optical Regeneration Scheme

Fig. 5.3 illustrates the schematic diagram of our proposed all-optical 16-QAM signal regeneration scheme. The basic idea of the 16-QAM signal regeneration scheme is to separate the information on X and Y quadrature of 16-QAM signal into two optical paths by using a PSA and to implement 2R regeneration separately. Incoming 16-QAM signal is split symmetrically into two partial signals, which are transmitted into two parallel arms, by a 50/50 splitter. Then each signal is regenerated by the following 2R regenerators, respectively. At the end, another 50/50 coupler is used to combine the two regenerated partial signals and the completed 16-QAM signal is restored as an output.

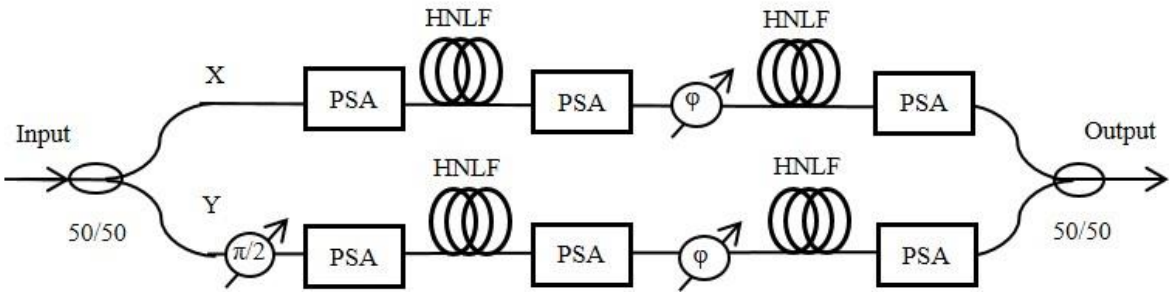

Fig. 5.3. Schematic diagram of all-optical 16-QAM signal regeneration scheme

In each arm, the first PSA following the coupler is used to amplify one quadrature of the incoming signal and to deamplify the other quadrature. Both the noise and the data encoded on the deamplified quadrature are erased by this PSA, leaving only the information encoded on the amplified quadrature. Hence, this arrangement effectively de-multiplexes X and Y quadrature. As shown in Fig. 5.3, the signal in the upper arm carries the data only from X-quadrature and the signal in the lower arm carries the data only from the Y-quadrature. Each signal contains two amplitude levels with power ratio of 1:9 plus the corresponding amplitude noise. Such de-multiplexing makes subsequent regeneration much easier in each arm. A variable phase delay is inserted in front of the second HNLF-PSA combination to optimize the regeneration performance. Then two 2R amplitude regenerators consisting of PSA and HNLF, as we discussed above, are implemented to suppress the amplitude noise on two amplitude levels with power ratio of 1:9. Similarly to the first PSA, the last PSA is use to squeeze some phase noise

introduced by the previous 2R regenerator. The last coupler restores the 16-QAM signals by combing regenerated X and Y quadrature signal at output.

5.3 Simulation results

In our simulation, the gains of the first, second and third PSAs in each arm are 13 dB, 10 dB, and 10 dB, respectively. The (nonlinear coefficient × fiber length) products are chosen so that the average SPM phase shifts induced by the first HNLF for higher power level and by the second HNLF for lower power level are both 0.65 rad. Loss and dispersion are neglected for simplicity. To quantify the regeneration performance, a normalized standard deviation (NSTD) $\delta = \sqrt{(\delta_X / X)^2 + (\delta_Y / Y)^2}$ is introduced, where X and Y are the mean values of X- or Y-quadrature amplitudes, and $\delta_{X,Y}$ are the standard deviations of X and Y, respectively. Obviously, the NSTDs are related to average power, meaning that, with the same amount of white noise, NSTDs at different power levels have a relationship of $\delta_1 = \sqrt{5}\,\delta_5$ and $\delta_1 = 3\delta_9$.

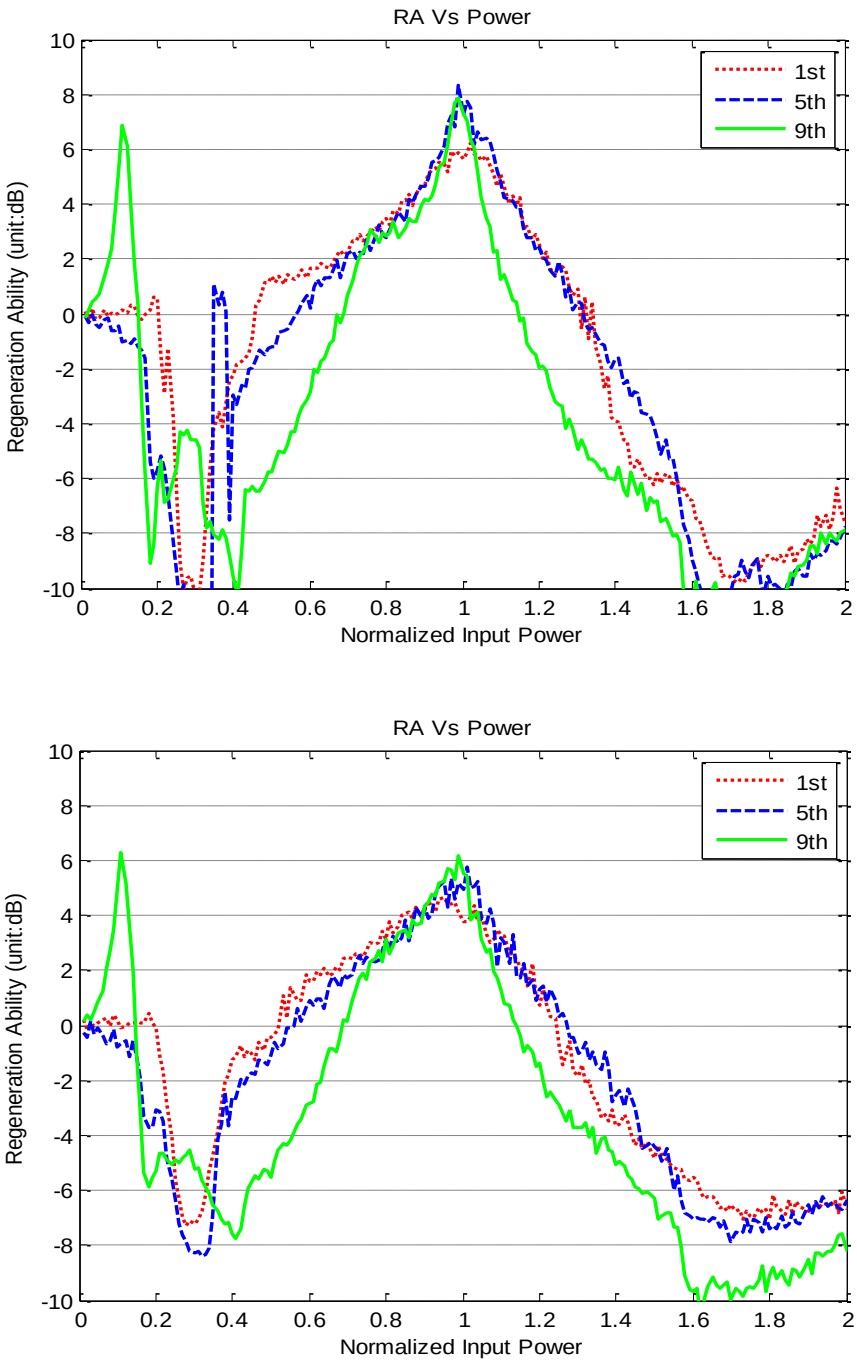

Fig. 5.4. RA of input with δ_9 = 1.5% (top) and δ_9 = 3% (bottom)

The ratio of the NSTDs of the input and output signals is defined as the regeneration ability (RA) [54], which is used to assess the performance of regenerators. Fig. 5.4 shows the RA for 16-QAM regeneration scheme versus input power with δ_9 = 1.5% (top) and δ_9 = 3% (bottom). The RA is optimized for the average input power for all three power levels. The dotted, dash and solid curves are for the 1st, 5th and 9th power level, respectively. After optimization, the optimum RA value for 1st, 5th and 9th power level is 6 dB, 8 dB and 8 dB when δ_9 is 1.5%, as well as 4 dB, 5 dB and 6 dB when δ_9 increases to 3%.

Figs. 5.5 and 5.6 shows constellation diagrams of the noise-degraded input and regenerated output signals of the 16-QAM regenerator. The input signal has high-power-level NSTD δ_9 = 1.5% in Fig. 5.5 and δ_9 = 3% in Fig. 5.6. The total number of symbols in the simulation is 1024. When the noise is relatively small (δ_9 = 1.5%), the regenerator performs a significant suppression on scattered signal points in the constellation. When the noise becomes large (δ_9 = 3%), the noise suppression is still obvious. However, in the latter case, output signal at the highest power level is regenerated better than at the lowest power level. This is because NSTD of the lowest power level is 9%, and this noise is too large to be reduced completely, which is consistent with the simulation result of RA above. Nevertheless, the better regeneration at the higher power level is actually beneficial because the nonlinear impairments in subsequent fiber spans come from the high-power levels.

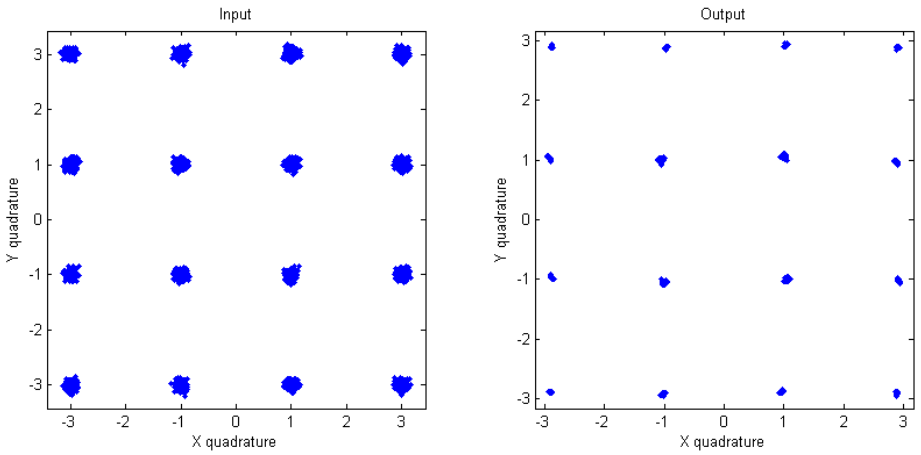

Fig. 5.5. Constellation diagrams of input (left) and output (right) with δ_9 = 1.5% for 16-QAM regeneration scheme

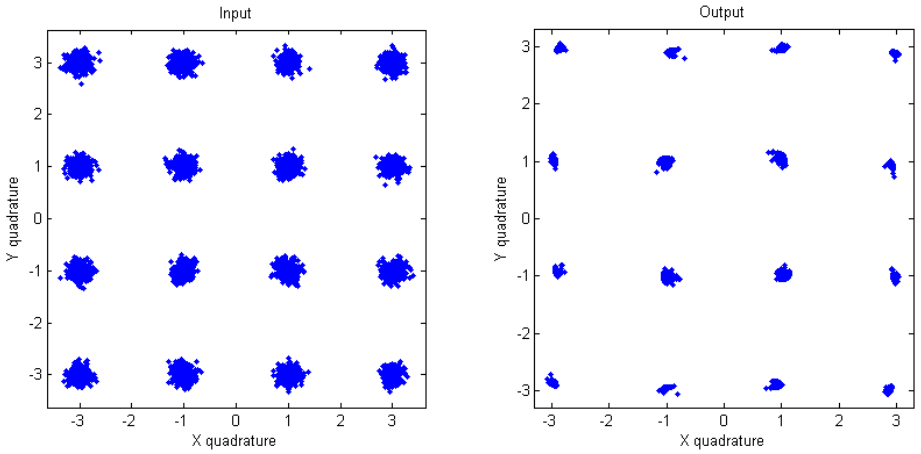

Fig. 5.6. Constellation diagrams of input (left) and output (right) with δ_9 = 3% for 16-QAM regeneration scheme

To summarize, we have proposed a novel all-optical scheme for 16-QAM signal regeneration based on PSA and new amplitude 2R regenerators. The first PSA is used to de-multiplex two quadratures and two cascaded amplitude 2R regenerators

in each arm are used to achieve two-level amplitude regeneration. In the numerical simulation, the capability of the regenerator has been demonstrated for the input 16-QAM signal with two different levels of white noise. The constellation results show that this scheme is able to regenerate both multi-level amplitude and phase simultaneously. The complex noise is reduced significantly through 16-QAM regeneration scheme when the NSTD δ_{9th} are 1.5% and 3%. Our scheme is potentially compatible with multi-channel operation, if the HNLF is replaced by the GDM medium, and the PSAs are operated in frequency-non-degenerate regime.

CHAPTER 6

CONCLUSIONS

This dissertation focuses on building a stand-alone multi-channel 2R regenerator based on GDM nonlinear medium and experimental demonstration of simultaneous 2R regeneration of multiple WDM channels. In addition, we also study the performance of DA-NOLM regenerator in experiments and propose a novel 16-QAM all-optical regenerator in simulation.

We have experimentally demonstrated, for the first time, to our knowledge, the simultaneous 2R regeneration of 100-GHz spaced 16 × 10 Gb/s WDM channels. This sets up two records: the highest number of simultaneously regenerated channels and the narrowest channel spacing. For this task, we have designed and built a novel GDM nonlinear medium consisting of several "fiber + PGDD" unit cells, bi-directionally pumped by Raman pump units. In our 3-channel experiments, 4 unit cells and 4 RPUs are used to achieve amplitude regeneration in both 100-GHz spacing and 200-GHz spacing cases. We have observed an eye-opening improvement greater than 2 dB and 3 dB for all 3 channels at 10^{-9} BER level in 100-GHz spacing and 200-GHz spacing cases, respectively. In our 100-GHz-spaced 12- and 16-channel experiments, a complete version GDM medium of 6 unit cells and 8 RPUs is employed to achieve optimized regeneration. We have observed an eye-opening improvement greater than 3 dB for all 12 channels at 10^{-8} BER level and greater than 5 dB for all 16 channels at 10^{-9} BER level.

In addition, we have also investigated a phase-preserving amplitude regenerator based on DA-NOLM for 50% duty-cycle RZ-DPSK signal regeneration. We have observed eye-opening improvement of 2.0 dB and 1.5 dB for a signal degraded by amplitude jitter only and a combination of ASE noise and amplitude jitter, respectively. By using the same DA-NOLM regenerator, we further demonstrated preventing of nonlinear amplitude-to-phase noise conversion of 50%-duty-cycle RZ-DPSK signal, resulting in 2-dB eye-opening improvement by employing a 40-km-long transmission link.

Furthermore, we have proposed, for the first time, to our knowledge, a novel all-optical scheme for 16-QAM signal regeneration, which is based on PSAs and new 2R regenerators. The PSAs are used for de-multiplexing two quadratures and phase noise suppression while the cascaded 2R regenerators are used for multi-level amplitude regeneration. The numerical results shows a significant regeneration on both amplitude and phase for all 16 states as well as robustness to variation in power.

In future, for a phase-encoded system, a phase-preserving amplitude regenerator with multi-channel capability will be needed. The NOLM regenerator considered above can be adapted to a multi-channel operation by replacing the HNLF with our GDM nonlinear medium [34]. For full phase regeneration, multi-channel PSAs can be used, based on non-degenerate FWM. For the phase-preserving regeneration of the remaining amplitude noisethe NOLM-based multi-channel 2R regenerators can be used. The 16-QAM regeneration scheme should be

further investigated and optimized. For example, replacing the 2R regenerator with NOLM that can do multi-level amplitude regeneration [55, 56] could simplify the setup and might improve the performance.

REFERENCES

[1] M. Vasilyev and T. I. Lakoba, "All-optical multichannel 2R regeneration in a fiber-based device," Opt. Lett. 20, 1458 (2005).

[2] P.V. Mamyshev, "All-optical data regeneration based on self-phase modulation effect," *24th European Conference on Optical Communication* (Institute of Electrical and Electronics Engineers, 1998), Vol.1, pp. 475−476.

[3] P. G. Patki, M. Vasilyev, and T. L. Lakoba, "All-optical regeneration of multi-wavelength signals," in *Proceedings of the IEEE LEOS European Winter Topical on Nonlinear Processing in Optical Fibres*, Innsbruck, Austria, January 12–14, 2009, paper WC2.3.

[4] P. G. Patki, M. Vasilyev, and T. L. Lakoba, "Multichannel all-optical regeneration," in *Proceedings of the IEEE Photonics Society Summer Topical Meeting on Nonlinear Fiber Optics*, Playa del Carmen, Mexico, July 19–21, 2010, paper WC2.2.

[5] E. Ciaramella, "Wavelength conversion and all-optical regeneration: achievements and open issues," J. Lightwave Technol. 30, 572–582 (2012).

[6] F. Parmigiani, et al. "Progress in multichannel all-optical regeneration based on fiber technology," IEEE J. Sel. Top. Quantum Electron. 18, 689–700 (2012).

[7] O. Leclerc, P. Brindel, S. Bigo, E. Brun-Maunand and E. Desurvire, "2×20Gbit/s, 3500 km regenerated WDM soliton transmission with all-optical Kerr fibre modulation," Electron. Lett. 34, 199–201 (1998).

[8] O. Leclerc, et al. "Simultaneously regenerated 4 × 40 Gbit/s dense WDM transmission over 10000 km using single 40 GHz InP Mach-Zehnder modulator," Electron. Lett. 36, 1574–1575 (2000).

[9] H. N. Tan, M. Matsuura, T. Katafuchi, and N. Kishi, “Multiple-channel optical signal processing with wavelength-waveform conversions, pulsewidth tunability, and signal regeneration,” Opt. Express 17, 22960–22973 (2009).

[10] G. Gavioli, and P. Bayvel, “Multichannel all-optical 3R regenerative wavelength conversion using an integrated semiconductor optical amplifier array,” In *Proceedings of the 16th Annual Meeting of the IEEE Lasers and Electro-Optics Society*, October 2003, vol. 2, pp. 896–897.

[11] Q. T. Le, et al. “WDM compatible 2R regeneration device based on eight-channel saturable absorber module,” Electron. Lett. 43, 1305 (2007).

[12] L. Bramerie, et al. “All-optical 2R regeneration with a vertical microcavity-based saturable absorber,” IEEE J. Sel. Top. Quantum Electron. 18, 870–883 (2012).

[13] K. Cvecek, et al. “Phase-preserving amplitude regeneration for a WDM RZ-DPSK signal using a nonlinear amplifying loop mirror,” Opt. Express 16, 1923–1928 (2008).

[14] T. Ohara, H. Takara, A. Hirano, K. Mori and S. Kawanishi, “40-Gb/s ×4-channel all-optical multichannel limiter utilizing spectrally filtered optical solitons,” IEEE Photon. Technol. Lett. 15, 763–765 (2003).

[15] L. Provost, F. Parmigiani, P. Petropoulos, and D. J. Richardson, “Investigation of simultaneous 2R regeneration of two 40-Gb/s channels in a single optical fiber,” IEEE Photon. Technol. Lett. 20, 270–272 (2008).

[16] P. Vorreau, et al. “Optical grooming switch with regenerative functionality for transparent interconnection of networks,” Opt. Express 17, 15173–15185 (2009).

[17] L. Provost, et al. “Investigation of four-wavelength regenerator using polarization- and direction-multiplexing,” IEEE Photon. Technol. Lett. 20, 1676–1678 (2008).

[18] C. Kouloumentas, et al. “Four-channel all-fibre dispersion-managed 2R regenerator,” IEEE Photon. Technol. Lett. 20, 1169–1171 (2008).

[19] N. S. Shah, and M. Matsumoto, “2R regeneration of time-interleaved multiwavelength signals based on higher order four-wave mixing in a fiber,” IEEE Photon. Technol. Lett. 22, 27–29 (2010).

[20] J. Wang, et al. “4×160-Gbit/s multi-channel regeneration in a single fiber,” Opt. Express 22, 11456–11464 (2014).

[21] N. Chi, L. Xu, K. S. Berg, T. Tokle, and P. Jeppesen, “All-optical wavelength conversion and multichannel 2R regeneration based on highly nonlinear dispersion-imbalanced loop mirror,” IEEE Photon. Technol. Lett. 14, 1581–1583 (2002).

[22] L. Li, M. Vasilyev, and T. I. Lakoba, “Investigation of 3-Channel All-Optical Regeneration in a Group-Delay-Managed Nonlinear Medium,” *the Conference on Lasers and Electro-Optics*, San Jose, CA, May 10–15, 2015, paper SM2M.2.

[23] L. Li, K. Young, C. Brandon, T. I. Lakoba and M. Vasilyev, “2R Regeneration of 12 WDM Channels with 100-GHz Spacing in a Group-Delay-Managed Nonlinear Medium,” *the Optical Fiber Communication Conference*, Anaheim, CA, March 20–24, 2016, paper W4D.4.

[24] L. Li and M. Vasilyev, “All-optical 2R regenerator of 16-QAM signals,” *the “Next-Generation Optical Communication: Components, Sub-Systems, and Systems III” conference* (part of SPIE OPTO / Photonics West), February 1–6, 2014, San Francisco, CA, paper 9009-7; Proc. SPIE 9009, 9009-7.

[25] Corning® SMF-28® ULL Optical Fiber

[26] T. Miya, Y. Terunuma, T. Hosaka, and T. Miyoshita, *Electron. Lett.* **15**, 106 (1979).

[27] M. Born and E. Wolf, *Principles of Optics*, 6th ed., Pergamon Press, Elmsford, NY, 1980.

[28] G. Agrawal, *Nonlinear Fiber Optics*, 4th ed., Academic Press, Burlington, MA, 2007.

[29] G. P. Agrawal, *Fiber Optic Communication Systems*, 3rd ed., Wiley & Sons, New York, 2002.

[30] A. G. Striegler, M. Meissner, K. Cvecek, K. Sponsel, G. Leuchs, and B. Schmauss, "NOLM-Based RZ-DPSK Signal Regeneration," IEEE Photon. Technol. Lett. **17**, 639 (2005).

[31] S. Boscolo, R. Bhamber, and S. K. Turitsyn, "Design of Raman-based nonlinear loop mirror for all-optical 2R regeneration of differential phase-shift-keying transmission," IEEE J. Quantum Electron. 42, 619 (2006).

[32] M. Matsumoto, "Performance improvement of phase-shift-keying signal transmission by means of optical limiters using four-wave mixing in fibers," J. Lightwave Technol. **23**, 2696 (2005).

[33] Q. T. Le, L. Bramerie, H. T. Nguyen, M. Gay, S. Lobo, M. Joindot, J.-L. Oudar, and J.-C. Simon, "Saturable-absorber-based phase-preserving amplitude regeneration of RZ DPSK signals," IEEE Photon. Technol. Lett. **22**, 887 (2010).

[34] T. I. Lakoba, J. R. Williams, and M. Vasilyev, "NALM-based, phase-preserving 2R regenerator of high-duty-cycle pulses," Opt. Express **19**, 23018 (2011).

[35] B. J. Eggleton, B. Luther-Davies, and K. Richardson, "Chalcogenide photonics," Nature Photon. 5, 141–148 (2011).

[36] D. J. Moss, R. Morandotti, A. L. Gaeta, and M. Lipson, "New CMOS-compatible platforms based on silicon nitride and Hydex for nonlinear optics," Nature Photon. 7, 597–607 (2013).

[37] C. K. Madsen, et al. "Integrated all-pass filters for tunable dispersion and dispersion slope compensation," IEEE Photon. Technol. Lett. 11, 1623–1625 (1999).

[38] C. R. Doerr, L. W. Stulz, S. Chandrasekhar, L. Buhl, and R. Pafchek, "Multichannel integrated tunable dispersion compensator employing a thermooptic lens," In *Proceedings of the Optical Fiber Communications Conference*, Anaheim, CA, March 17–22, 2002, paper PDFA6.

[39] N. Stelmakh, and M. Vasilyev, "Multiport AWG-based dispersion compensators," In *Proceedings of the IEEE Photonics Society Summer Topical Meeting on Novel Waveguiding, Structures, and Phenomena*, Playa del Carmen, Mexico, July 19–21, 2010, paper WB2.5.

[40] G. Belotti, and S. Bigo, "Cross-phase modulation suppressor for multispan dispersion-managed WDM transmissions," IEEE Photon. Technol. Lett. 12, 726–728 (2000).

[41] G. Bellotti, S. Bigo, P. Y. Cortès, S. Gauchard, and S. LaRochelle, "10×10 Gb/s Cross-phase modulation suppressor for multispan transmissions using WDM narrow-band fiber Bragg gratings," IEEE Photon. Technol. Lett. 12, 1403–1405 (2000).

[42] X. Wei, X. Liu, C. Xie, and L. F. Mollenauer, "Reduction of collision-induced timing jitter in dense wavelength-division multiplexing by the use of periodic-group-delay dispersion compensators," Opt. Lett. 28, 983–985 (2003).

[43] L. F. Mollenauer, et al. “Experimental test of dense wavelength-division multiplexing using novel, periodic-group-delay-complemented dispersion compensation and dispersion-managed solitons,” Opt. Lett. 28, 2043–2045 (2003).

[44] T. I. Lakoba and M. Vasilyev, “A new robust regime for a dispersion-managed multichannel 2R regenerator,” Opt. Express 15, 10061–10074 (2007).

[45] C. Kouloumentas et al, “Four-Channel All-Fiber Dispersion-Managed 2R Regenerator,” IEEE PTL 20, 1169 (2008).

[46] M. Vasilyev, M. Mehendale, and S. Tsuda, “Optimum pre-emphasis in ultralong-haul networks,” in *Journal of Optical Networking,* Vol.5, pp.159-174, March 2006.

[47] J. P. Gordon and L. F. Mollenauer, “Phase noise in photonic communication systems using linear amplifiers,” Opt. Lett., 15, 1351 (1990).

[48] A.H. Gnauck, P.J. Winzer “Optical phase-shift-keyed transmission,” J. Lightwave Technol. 23, 115–130 (2005).

[49] Z. Zheng, L. An, Z. Li, X. Zhao, X. Liu, “All-optical regeneration of DQPSK/QPSK signals based on phase sensitive amplification,” Opt. Commun. 281(10), 2755–2759 (2008).

[50] K. Croussore, I. Kim, Ch. Kim, Y. Han, G. Li, “Phase-and-amplitude regeneration of differential phase-shift keyed signals using a phase-sensitive amplifier,” Opt. Express 14, 2085–2094 (2006).

[51] R. Slavik, et al “All-optical phase and amplitude regenerator for next-generation telecommunications systems”, Nature Photonics 4, 690-695 (2010).

[52] J. Kakande, A. Bogris, R. Slavik, F. Parmigiani, D. Syvridis, P. Petropoulos, D. J. Richardson, "First demonstration of all-optical QPSK signal regeneration in a novel multi-format phase sensitive amplifier," *ECOC 2010*. postdeadline paper 3.3, pp. 1-3.

[53] K. Croussore, G. Li, "Phase regeneration of NRZ-DPSK signals based on symmetric-pump phase-sensitive amplification," IEEE Photon. Tech. Lett. 19, 864–866 (2007).

[54] K. Cvecek, K. Sponsel, G. Onishchukov, B. Schmauss, G. Leuchs, "2R-Regeneration of a RZ-DPSK signal using a nonlinear amplifying loop mirror," IEEE Photon. Technol. Lett. 19, 146-158 (2007).

[55] M. Hierold, T. Roethlingshoefer, K. Sponsel, G. Onishchukov, B. Schmauss, G. Leuchs, "Phase-preserving Multilevel Amplitude Regeneration Using a Modified Nonlinear Amplifying Loop Mirror" *ICTON 2010*, paper Mo.B1.6.

[56] M. Hierold et al "Multilevel phase-preserving amplitude regeneration using a single nonlinear amplifying loop mirror," IEEE Photon. Technol. Lett. 99, (2011)

BIOGRAPHICAL INFORMATION

Lu received his Bachelor of Science degree in Opto-electronics Science and Technology from Nankai University, Tianjin, China and his Master of Science degree in Opto-electronics Technology from Tianjin University, Tianjin, China. He joined UTA in 2010. He was vice-president of Optical Society of America (OSA) student chapter for 2013 – 2016 at UTA. His research interests include all-optical signal processing, nonlinear optics, and fiber-optic communications.